Alma Mater Studiorum – Università di Bologna

DOTTORATO DI RICERCA IN
ONCOLOGIA, EMATOLOGIA E PATOLOGIA

Ciclo 34

Settore Concorsuale: 06/D3 - MALATTIE DEL SANGUE, ONCOLOGIA E REUMATOLOGIA

Settore Scientifico Disciplinare: MED/06 - ONCOLOGIA MEDICA

Comprehensive characterization of SDH-deficient GIST using NGS data and iPSC models

Presentata da: Angela Schipani

Coordinatore Dottorato

Prof.ssa Manuela Ferracin

Supervisore

Prof.ssa Maria A. Pantaleo

Co-supervisore

Dott.ssa Annalisa Astolfi

Esame finale anno 2022

CONTENTS

ABSTRACT

Gastrointestinal stromal tumors (GIST) are the most common di tumors of the gastrointestinal tract, arising from the interstitial cells of Cajal (ICCs) or their precursors[1]. The vast majority of GISTs (75–85% of GIST) harbor KIT or PDGFRA mutations[2-3]. A small percentage of GIST (about 10-15%) do not harbor any of these driver mutations and have historically been called wild-type (WT). Among them, from 20% to 40% show loss of function of the succinate dehydrogenase complex (SDH), also defined as SDH-deficient GIST[4]. SDH-deficient GISTs display distinctive clinical and pathological features, and can be sporadic or associated with Carney triad or Carney-Stratakis syndrome[5,6,7]. These tumors arise most frequently in the stomach with predilection to distal stomach and antrum, have a multi-nodular growth, display a histological epithelioid phenotype, and present frequent lympho-vascular invasion. Occurrence of lymph node metastases and indolent course are representative features of SDH-deficient GISTs. This subset of GIST is known for the immunohistochemical loss of succinate dehydrogenase subunit B (SDHB), which signals the loss of function of the entire SDH-complex[2]. The overall aim of my PhD project consists of the comprehensive characterization of SDH deficient GIST. Throughout the project, clinical, molecular and cellular characterizations were performed using next-generation sequencing technologies (NGS), that has the potential to allow the identification of molecular patterns useful for the diagnosis and development of novel treatments. Moreover, while there are many different cell lines and preclinical models of KIT/PDGFRA mutant GIST, no reliable cell model of SDH-deficient GIST has currently been developed, which could be used for studies on tumor evolution and in vitro assessments of drug response. Therefore, another aim of this project was to develop a pre-clinical model of SDH deficient GIST using the novel technology of induced pluripotent stem cells (iPSC).

INTRODUCTION

1. Gastrointestinal stromal tumor (GIST)

Gastrointestinal stromal tumors (GISTs) are the most common mesenchymal tumors of the gastrointestinal tract, with an estimated annual incidence of around 1 case in 100 000[8,9]. GISTs are an heterogenous group of disease in both the clinical presentation and molecular background. The reported median age at diagnosis is 66–69 years and the ratio of men to women is approximately equal. Much less commonly, GISTs can occur in the pediatric population with an higher female incidence[10]. Most of GISTs are sporadic, however GISTs have also been identified in association with neurofibromatosis type 1 (NF1), characterized by a germline mutation of the NF1 gene; Carney triad syndrome, marked by hypermethylation of SDHC gene of the SDH complex and Carney-Stratakis syndrome, characterized by a germline mutation in one of the subunit (A, B, C and D) genes of the SDH enzyme complex[5,6,7]. GISTs share morphological and immunophenotypic features with the interstitial cells of Cajal (ICC). These mesenchymal cells are the functional intermediaries between the autonomic nervous system and smooth muscle cells, and promote the autonomous peristaltic contractions of the gut. In particular, GISTs, alike Cajal cells, are almost uniformly KIT-expressing, therefore they are thought to originate from the ICC[1].

1.1. Clinical and pathological manifestations of GISTs

GISTs are most commonly found in the stomach (50%–60%) and small intestine (30%–35%) and are less frequently found in the colon and rectum (5%) and the esophagus (1%)[11]. Microscopically, GISTs may present moderate or high cellularity and can be composed of three main cell types: spindle (70%), epithelioid (20%) or mixed (10%)[12]. From an immunohistochemical point of view, GISTs are mostly characterized by the expression of two specific markers, KIT (CD117) and DOG-1. Other markers are the protein kinase C theta (PKC-theta), CD34, smooth muscle actin, S-100 protein, desmin and keratin[13]. Clinically, small size GISTs are usually asymptomatic and they are diagnosed incidentally on abdominal CT scans, during endoscopy or during surgery[14]. Symptomatic patients may present nonspecific symptoms such as early satiety, vomiting, anemia, abdominal pain, swelling[15,16]. On the other hand, large tumors may cause abdominal distention, obstruction of the gastrointestinal lumen (tumors with endophytic growth) or compression of the gastrointestinal tract

(GISTs with exophytic growth). Esophageal GISTs present dysphagia as first specific symptom. Furthermore, in advanced stages, metastases can occur, however a significant number of patients presents metastases at the time of diagnosis because of the diagnosis delay[17]. Most often, metastases are localized in the liver (65%) and peritoneum (21%) and rarely, in bones, lungs and lymph nodes[12].

1.2. Molecular classification of GISTs

Most GISTs (75–85% of GISTs) harbour the driver mutations in the tyrosine kinase receptor KIT and/or platelet-derived growth factor receptor-α (PDGFR-α) leading to malignant transformation through the activation of the growth factor receptor signalling pathways[2-3]. KIT and PDGFRA genes both encode structurally similar tyrosine kinase receptors. These receptors are composed of an extracellular ligand-binding region, a transmembrane sequence, a juxtamembrane domain and two cytoplasmic kinase domains[18,3]. In GISTs, mutations in KIT and PDGFRA genes mostly involve either the cytoplasmic kinase domain or the juxtamembrane (intracellular or extracellular) regions[19,20]. The vast majority of KIT mutations are found in exon 11 (∼70%) and in exon 9 (∼10%), whereas the most common PDGFRA mutations occur in exon 18. These primary mutations are mutually exclusive so that primary tumors have either a KIT or a PDGFRA mutation but not both[21,22]. A small subset of GISTs (∼10-15%) lacks such oncogenic mutations and have historically been classified as wild-type GISTs (WT). Subgroups of KIT/PDGFRA WT (∼15%) are driven by mutations in BRAF/RAS or NF1 altogether involving the RAS-pathway (RAS-P). Conversely, from 20% to 40% show the loss of function of the succinate dehydrogenase complex (SDH), also defined as SDH-deficient GIST[23,24,4]. The remaining 50% of cases, accounting for about 5% of all GIST, do not carry any mutations in KIT/PDGFRA/SDH/RAS-P genes and consequently, are usually called quadruple WT (qWT) GIST [25,26] (Figure 1).

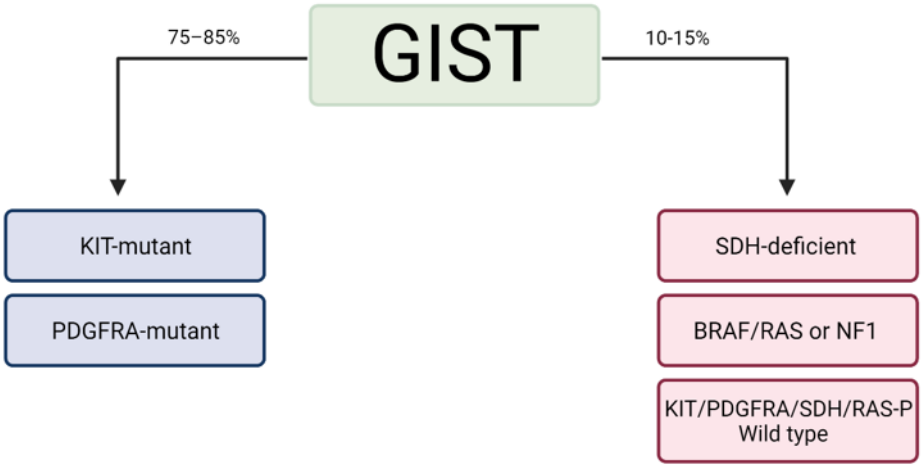

Figure 1.**Molecular classification of GISTs.**

1.3. Risk stratification and treatments

Since all GISTs can be considered malignant, several criteria of risk stratification have been developed over the years. Clinically, the classification scores by Fletcher et al., and Miettinen and Lasota are the most generally accepted[27,28,29]. Fletcher et al. classify the risk of aggressive evolution in four groups, depending on tumour size and mitotic rate[27]:

Table 1.**Risk stratification of GISTs based on tumour size and mitotic count.**

Risk stratification	Tumor Size (cm)	Mitotic count
Very low	<2	<5/50 high-power field(HPF)
Low	2-5	<5/50 HPF
Intermediate	<5 or 5-10	6-10/50 HPF <5/50 HPF
High	>5 or >10	>5/50 HPF >10/50 HPF

Mutational status has not been incorporated in any risk classification at present, although some genotypes have peculiar clinical presentations and clinical course. For example, among mutated GISTs, those with D842V PDGFRA mutation are generally associated with a good prognosis. On the contrary, KIT exon 11 deletions involving codons 557-558 have been repeatedly reported to be associated with a high risk for relapse[30]. With regards to GISTs treatment, traditional chemotherapy and radiation are not effective on GISTs. The standard treatment for non-metastatic GISTs is

surgery. Most metastasis of GISTs are liver metastasis or peritoneal seeding, and lymph node metastasis is extremely rare, so lymph node dissection is not recommended[12]. The goal in primary GISTs is the complete removal (R0) that can be achieved with both the tumor and its pseudocapsule removal[28]. GISTs with high risk of recurrence or even metastasis require the adjuvant therapy with tyrosine kinase inhibitors (TKIs). The introduction of TKIs has significantly improved extending recurrence-free survival after surgery[31] and prolonging overall survival in metastatic or unresectable cases[32]. The targeted TKI imatinib is typically the selected first treatment for most advanced, unresectable and metastatic patients. Sunitinib (second-line tyrosine kinase inhibitor)[33] and regorafenib (third-line multikinase inhibitor)[34] can be used in advanced GISTs after treatment failure with imatinib. However, it is difficult to obtain a permanent cure by tyrosine kinase inhibitors. Therefore, early diagnosis (early GISTs without metastasis) with early surgical resection is the only promising way to obtain complete cure of this disease[35].

2. Succinate dehydrogenase (SDH) complex

Succinate dehydrogenase, SDH, is a mitochondrial enzyme complex (also known as complex II of the electron transport chain) that is involved in both the citric acid cycle and the electron transport chain. In particular, complex II couples the oxidation of succinate to fumarate in the Krebs cycle with the electron transfer to the terminal acceptor ubiquinone in the electron transport chain. The assembled SDH complex, located into the inner membrane of the mitochondria, consists of four-subunits encoded by nuclear genes (SDHA, SDHB, SDHC, and SDHD, collectively indicated to as SDHx)[36]. The flavoprotein and succinate-binding SDHA, and the iron-sulfur protein SDHB are the catalytic subunits of the complex, responsible for the conversion of succinate to fumarate and ubiquinone to ubiquinol respectively; while SDHC and SDHD are the anchoring components that attach the SDH to the inner mitochondrial membrane. All of the SDH genes are involved in the tumorigenesis of different types of cancers including GIST, paraganglioma, pheochromocytoma, renal cell carcinoma, Hodgkin lymphoma, chronic lymphocytic leukemia, thyroid cancer, pituitary adenomas, and neuroendocrine tumors of the pancreas[37].

3. Succinate dehydrogenase (SDH)–deficient GISTs

3.1. Clinical presentations

Succinate dehydrogenase (SDH)–deficient GISTs are the largest group of KIT/PDGFRA WT GISTs and the only group of GISTs characterized by an energy metabolism defect as the key oncogenic mechanism[38]. Loss of function of the succinate dehydrogenase complex mainly characterizes the SDH-deficient GISTs. SDH-deficient GISTs are easily recognized by clinical and pathological features that are peculiar to this subtype. They arise most frequently in the stomach with predilection to distal stomach and antrum, and frequently exhibit lymph vascular invasion. Occurrence of lymph node metastases and indolent course are representative features of SDH-deficient GISTs and may sometimes be fatal. SDH-deficient GISTs are relatively small with a low mitotic activity (<5 mitoses/5 mm^2)[39]. They are usually indolent and a small proportion of them metastasizes to the liver, often after a long delay of 10 years or more after its initial development. The apparent slow growth of the SDH-deficient GISTs can be supposed to be related to the metabolic deficit provided by the loss of function of the complex II of the mitochondrial chain[40]. Clinical manifestations that lead to the detection of SDH-deficient GISTs are similar to those of other gastric tumors, like gastrointestinal bleeding and epigastric discomfort[39]. They generally tend to develop in children and young patients and can be sporadic or associated with Carney-Stratakis syndrome and Carney triad. Carney-Stratakis syndrome is a rare hereditary condition characterized by multifocal paragangliomas and GIST. On the other hand, Carney triad is a rare non-hereditary disease cause by the association of GIST, pulmonary chondroma and paraganglioma[41,6,42].

3.2. Pathological features

This subset of GIST is known for the immunohistochemical loss of succinate dehydrogenase subunit B (SDHB), which signals the loss of function of the entire SDH-complex. SDHB protein expression on immunohistochemistry is a diagnostic marker for loss of function of the SDH complex, whereas SDHA immunohistochemistry is able to identify SDHA-mutant GISTs[43]. SDH-deficient GISTs are uniformly immunohistochemically positive for KIT and DOG1/Ano1 (Anoctamin-1). Histologically SDH-deficient GISTs show a multi-nodular growth, forming tumour nodules between strands of gastrointestinal smooth muscle, which has been referred to as plexiform pattern. The tumour cells display an histological epithelioid or mixed spindled/epithelioid phenotype.

Tumour size is varied, with most cases ranging from 1.5 to 12 cm (median, 5.0 cm). Mitotic rate may reach more than 5x5 mm^2, and occasionally atypical mitoses can be seen[44].

3.3. Molecular analysis

Tumour development caused by SDH-deficiency results from the complete loss of function of one SDHx subunit, the entire SDH complex becomes unstable and the enzymatic function of the SDH complex is lost. SDH-deficiency can be caused by different genetic mechanisms. In most of SDH-deficient GISTs the loss of function of the complex is due to the presence of mutations in one subunit of the complex. Normally, the combination of a first hit, that is an inactivating germline mutations, with a second hit, represented by other inactivating mutation affecting the second allele or somatic loss of heterozygosity, leads to the loss of function of an SDHx subunit. Less frequently, SDH deficiency is caused by the somatic inactivation of both alleles of a given complex subunit or SDH assembly factor[45]. Approximately half of patients with SDH-mutated GISTs have mutations in one of the SDH subunits and SDHA mutations are the most common (30%) with resultant loss of SDHA and SDHB protein expression immunohistochemically[8]. The majority of these cases are germline mutations. SDHA patients usually carry two mutational events at the SDHA locus, either the loss of the wild type allele or a second somatic event in compound heterozygosis[46,47,48,49]. SDHB, SDHC, and SDHD mutations in GIST occur in only 20%–30% of cases and most of these SDH mutations are germline. Approximately 20% of those showing these SDH subunit mutations also have paragangliomas[4,50]. The remaining 50% of the SDH-deficient GIST lack SDHx mutations, and are instead caused by an hypermethylation of the SDHC promoter, which leads to the repression of SDHC transcription and depletion of SDHC protein levels, through a mechanism described as epimutation. SDH-deficient GISTs are characterized by a lack of immunohistochemical expression of the SDHB protein independently of the mutant subunit [51,52].

3.4. Biochemical consequences of SDH complex deficiency

Disruption of the SDH complex, caused by either biallelic loss-of-function mutations or epigenetic inactivation, leads to the accumulation of succinate, an oncometabolite that promotes tumorigenesis by activating different pathways (Figure 2). Accumulation of succinate inhibits the activity of prolyl-hydroxylase domain proteins (PHD) leading to the stabilization of hypoxia inducible factor 1

(HIF1). Generally, PHD regulate the oxygen dependent hydroxylation of the HIF-α, leading to their polyubiquitination and proteasomal degradation[53]. The inactivation of PHD creates a pseudo-hypoxia state, causing the stabilization of HIF-α, which in turn leads to increased expression of the transcriptional factors as vascular endothelial growth factor (VEGF) and insulin-like growth factor-1 (IGF1) causing increased angiogenic and cell growth signalling. These tumours are characterized by an overexpression of IGF-1 receptor (IGF1R) both at the mRNA and protein level without IGF1R genomic amplification[54,55,56]. Moreover, the accumulation of succinate, that is structurally similar to α-ketoglutarate (α-KG), leads to the inhibition of the α-KG dependent dioxygenases such as JmjC domain containing histone lysine demethylases (KDM) and ten–eleven translocation (TET) enzymes. The latter are involved in DNA demethylation and transcriptional silencing because they drive the active removal of 5-methylcytosine (5mC) from methylated CpG sites. Consequently, genome-wide DNA hypermethylation may be related to the disruption of DNA demethylation machinery by downregulated TET enzyme[57]. Intriguingly, it has been recently shown that the characteristic hyper-methylation in these tumors is associated with changes in genome topology that can drive oncogenic program. The hyper-methylation is associated with pervasive insulator losses and topological reorganization of the FGF and KIT loci. In particular, the hypermethylated phenotype disrupts the binding of CTCF in regions located in proximity to the FGF3/FGF4 locus, causing FGF4 overexpression[58].

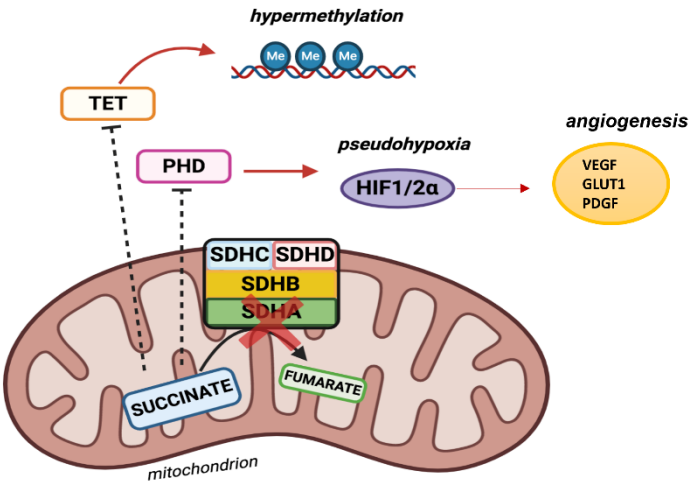

Figure 2.**Schematic representation of SDH complex.** The figure shows the functional consequences of the loss of function. HIF, hypoxia-inducible factor; Me, methyl group; PHD, prolyl-hydroxylase domain proteins; SDH, succinate dehydrogenase; TET, ten–eleven translocation. VEGF,vascular-endothelial growth factor; GLUT1, glucose transporter protein type 1;PDGF, platelet-derived growth factor. Modified from Nannini et al, Ther Adv Med Oncol. 2021 Jun 28.

3.5. Treatment of SDH-deficient GISTs

Both KIT/ PDGFRA mutant and WT GISTs do not respond to traditional cytotoxic chemotherapy. The introduction of tyrosine kinase inhibitor (TKIs) revolutionized the treatment of KIT and PDGFRA TKI-sensitive mutations. However, SDH-deficient GISTs poorly respond to treatment with imatinib because of the lack of activating tyrosine kinase mutations, but tend to better respond to the inhibitors of the angiogenesis[59]. Indeed, the loss of function of the SDH complex drives an increased signalling of the vascular endothelial growth factor receptor (VEGFR) and insulin growth factor receptor (IGF1R) via the hypoxia-inducible factor 1a transcriptional activity. Both VEGFR and IGF1R are targets of sunitinib[11,55], an inhibitor of angiogenesis. Another oral, multi-kinase inhibitor is regorafenib, that has inhibitory effects on several protein kinases, including those involved in angiogenesis (VEGFR1, VEGFR2, VEGFR3, and TIE3)[60,34]. These angiogenetic inhibitors, sunitinib and regorafenib, are approved as second-and third-line treatments in patients with GIST who develop resistance to imatinib. Other inhibitors have been tested, such as Pazopanib, KIT, VEGFR-1, VEGFR-2, VEGFR-3, and PDGFR inhibitor[61]; Nilotinib, which shows activity against BCR-ABL kinases, discoidin domain receptor (DDR), KIT, PDGFR, and colony-stimulating factor receptor-1 (CSF-1R)[62,63]; Lisitinib is an inhibitor of IGF1R[64]; Vandetanib, another oral inhibitor of epidermal growth factor receptor (EGFR), VEGFR, and RET[65]. Surgery is anyway the most important treatment approach for nonmetastatic KIT/PDGFRA WT GIST and is recommended by the National Comprehensive Cancer Network[66].

AIM OF THE STUDY

SDH-deficient GIST is a small subgroup of a rare tumour and therefore a complete study of this disease results in numerous challenges. Large, randomised clinical trials are often impractical because they are rare and poorly characterised. Based on these considerations, the overall aim of this PhD project consisted on the comprehensive characterization of SDH-deficient GISTs. The use of next-generation sequencing technologies aimed to assess the molecular characteristics of this subgroup. This allowed for the identification of altered pathways that can be used in the diagnosis and development of new treatments. Moreover, the germline mutational analysis intended to investigate and confirm distinct features of SDHA-deficient GIST patients. The germinal molecular analysis of a group of SDHA-patients is necessary for the understanding of the hereditary components of the disease and its clinical implication. Finally, we focused on the development of a cell model to reproduce in vitro a disease model that can be used to deeply study the biomolecular characteristics of this type of disease and to mainly test new therapeutic approaches. Moreover, the development of an SDH-deficient GISTs model could have a big impact on the study of other tumours with deficit of the SDH complex. The information gained from studying this model might also lead to an increased understanding of other tumour types and could allow to improve existing treatments.

MATERIALS AND METHODS

1. Patients

Sixteen SDHA-mutant GISTs were enrolled in SDHA germline study. All cases presented gastric localisation of the tumor and negative immunohistochemistry for SDHB. The tumor and patient's characteristics are summarized in Table 2.

Table 2.**Patients and tumor characteristics**. AWD, Alive with disease; AWOD, Alive without disease; DOD, Died of disease; NA, Not available.

Pts N°	Age	Gender	Primary site	Multifocality	Disease Status at diagnosis	Follow up time	Patient status
#1	28	F	stomach	yes	metastatic	15.8 yrs	AWD
#2	30	M	stomach	no	metastatic	13.0 yrs	AWOD
#3	31	F	stomach	no	localized	7.4 yrs	AWOD
#4	61	M	stomach	no	localized	3.3 yrs	AWOD
#5	21	F	stomach	yes	localized	22.8 yrs	AWOD
#6	39	F	stomach	no	metastatic	14.7 yrs	AWD
#7	37	F	stomach	no	localized	9.6 yrs	AWOD
#8	38	M	stomach	no	localized	5.0 yrs	AWOD
#9	70	F	stomach	no	localized	10.0 yrs	AWOD
#10	66	F	stomach	no	localized	2.2 yrs	AWD
#11	17	M	stomach	no	localized	22.7 yrs	AWD
#12	55	F	stomach	no	metastatic	12.0 yrs	DOD
#13	50	M	stomach	no	localized	9.6 yrs	AWOD
#14	17	M	stomach	no	localized	4.8 yrs	AWOD
#15	54	F	stomach	NA	NA	NA	NA
#16	18	F	stomach	yes	localized	NA	NA

Regarding the gene expression and immune profile, thirty-six GISTs tumour samples, from either formalin-fixed, paraffin-embedded (FFPE) by microarray or from fresh frozen tissue by RNAseq were retrospectively collected among KIT-mutant (29 cases) and SDH-deficient GISTs (7 cases). FFPE samples were obtained by fixing the surgical specimens in 10% NBF (formalin solution, neutral buffered) for 6 h, then dehydrated and included in paraffin. Fresh frozen tissue specimens were collected during the surgical operation, snap-frozen in liquid nitrogen, and stored at -80 °C until RNA extraction. The mutational status of all the samples were assessed by using Sanger

sequencing. Moreover, the SDH-deficient status was evaluated by immunohistochemistry of the SDHB subunit. Patients' data are reported in Table 3.

Table 3.**GIST patients' features stratified by succinate dehydrogenase deficiency (SDH deficient) and proto-oncogene c-Kit mutant (KIT-mutant).** *High power fields. ** GIST010 and GIST007 with both platforms.

Parameters	SDH deficient n=7	KIT mutant n=29
Sex		
Female	4	11
Male	3	18
Age (average,range)	25 (18-30)	62.4 (34-87)
Site		
Intestine	0	9
Stomach	6	17
NA	1	3
Tumor size		
< 5 cm	0	4
≥ 5 cm	5	22
NA	2	3
Mitotic rate		
< 5 /50 HPF	0	9
≥ 5 /50 HPF	4	15
NA	3	5
Desease status at diagnosis		
Localized	0	18
Metastatic	5	7
NA	2	4
Platform		
Microarray	4**	21
RNA-seq	5**	8

Regarding the cell model, iPSC have been generated from the peripheral blood mononuclear cells (PBMCs) of one SDH-deficient patient carrying a germline mutation c.1766 G>A, R589Q, in heterozygosity, at the level of exon 13 of SDHA subunit. The study was performed in accordance with the Declaration of Helsinki protocols.

The studies were reviewed and approved by the local Institutional Ethical Committee of Azienda Ospedaliero-Universitaria Policlinico S.Orsola-Malpighi, Bologna, Italy (approval number 113/2008/U/Tess and 1060/2020/Sper/AOUBo) and informed consent was provided by all living patients.

2. Sequencing of SDHA-deficient GISTs

For germline analysis, DNA was extracted from peripheral blood or FFPE normal tissue with the QiaAmp mini or micro kit (Qiagen). For somatic analysis, manual macrodissection of the tumor area was performed using a scalpel on areas selected by an expert pathologist on FFPE slides. At least 70% tumor enrichment was required for sample inclusion, and DNA was extracted using QiaAmp micro kit. SDHA variants were identified by Sanger sequencing; following the amplification of the exonic and flanking intronic regions of SDHA using FastStart TAQ polymerase (Roche), the samples were sequenced using the Big Dye Terminator v1.1 Cycle Sequencing kit (Applied Biosystems) on ABI 3730 Genetic Analyzer (Applied Biosystems). Primer pairs were designed with Primer Express 3.0 Software (Applied Biosystems) to specifically amplify SDHA exons and not the related pseudogenes[4]. Germline mutational analysis was performed on peripheral blood in nine cases and on matched normal tissue extracted from FFPE in five cases. Unfortunately, in two cases the matched normal counterpart was not available. Allele frequency in the general population was reported from the Genome Aggregation Database (gnomAD) v2.1.1, reporting data from 141,456 individuals. Variant classification was performed following ACMG recommendations using the VarSome shared data resource (https://varsome.com/).

3. Gene expression and immune profile

Total RNA extraction was performed by using the RNeasy Mini Kit (Qiagen, Milan, Italy) and then processed to be analysed either on HGU133Plus 2.0 Affymetrix microarrays or by whole-transcriptome RNA sequencing on Illumina platform. Briefly, for microarray samples, quality-controlled RNA was labelled following the Affymetrix manufacturer's recommendations and then hybridized to HGU133Plus 2.0 arrays. Gene expression data were normalized and quantified as log2signal by the robust multichip average (RMA) algorithm (package oligo, R-bioconductor). For the RNAseq analysis, the cDNA libraries were synthesized starting from 250 ng total of RNA with TruSeq RNA Exome (Illumina, San Diego, CA, USA) according to the manufacturer's protocol. Sequencing by synthesis was performed on Nextseq500 sequencer (Illumina) at 75 bp in paired-end mode.

3.1. Bioinformatics analysis

An average of 49.5 million reads per sample were obtained, reaching an average coverage of ~45X. Read pairs were mapped on reference human genome hg38 with STAR (https://github.com/alexdobin/STAR accessed 15 October 2020), duplicates removed, and sorting and indexing were performed with samtools (http://www.htslib.org/ accessed 15 October 2020). Gene expression was quantified and normalized in two different ways: (1) as count per million (CPM) by adopting the python package HTseq-count to get the raw count (https://htseq.readthedocs.io/ accessed 15 October 2020), followed by the R-bioconductor package edgeR to compute the normalization factors (https://bioconductor.org/packages/release/bioc/html/edgeR.html accessed 15 October 2020); (2) as transcript per million (TPM) using the program kallisto (https://pachterlab.github.io/kallisto accessed 15 October 2020). The two normalization methods are conceptually different and suited to perform different types of downstream analysis; generally CPM are employed to compare between samples while TPM are best suited to compare between genes[67]. Here, CPM was used to perform the principal component analysis (PCA) and the evaluation of differential expression (DE), and the TPM values were considered to estimate the tumor microenvironment composition and to quantify the gene signatures. The R package prcomp (https://cran.r-project.org/package=nsprcomp accessed 15 October 2020) was used to perform the PCA, and the three-dimensional projections, corresponding to the first three components, were plotted with the function plot3d of rgl package (https://cran.r-project.org/package=rgl accessed 15 October 2020). The DE analysis of SDH-deficient versus KIT-mutant GISTs was performed by using the R-bioconductor limma package (https://www.bioconductor.org/packages/release/bioc/html/limma.html accessed 15 October 2020), sequentially adopting the functions lmFit (to produce a fitted model) and eBayes (to compute moderate t-statistic and log2 fold change). Significantly modulated genes (over- or underexpressed) were defined on the basis of q-value < 0.05 (adjustment method Benjamini–Hochberg). The methods described for PCA and DE was applied to both microarray and RNA-seq data series. Over-representation analysis was performed separately for over- and underexpressed gene lists to determine whether genes associated to a specific pathway are present more than expected. The web tool Enrich (https://maayanlab.cloud/Enrichr/ accessed 15 October 2020) was used focusing on MSigDB Hallmark 2020 to evaluate pathways and Human Gene Atlas to evaluate cell type. As input, two lists of up- and down-regulated genes, obtained by the consensus between microarray or

RNA-seq DE results, were entered. It was included significantly modulated genes (q-value < 0.05) in microarray data having the same fold change sign and p-value < 0.01 in RNA-seq analysis (and vice versa). Gene set enrichment analysis (https://www.gsea-msigdb.org/gsea/index.jsp accessed 15 October 2020) was performed adopting the full expression matrix (without any filter) for both microarray and RNA-seq data. The Gene Set Enrichment Analysis (GSEA) was run by selecting the curated gene set carrying "canonical pathways" from Molecular Signatures Database (MSigDB) and adopting the following parameters: number of permutation = 100; enrichment statistic = "classic"; metric for ranking gene = "Diff_of_Classes"; normalization mode = "meandiv". A tumor microenvironment study was performed by using CIBERSORT, and immuno-related gene signatures were evaluated as previously described[68].

4. Reprogramming adult cells in iPSC

The reprogramming of PBMCs into iPSC was performed with CytoTune™-iPS 2.0 Sendai Reprogramming Kit (ThermoFisher) using vectors based on a modified, non-transmissible form of Sendai virus (SeV) encoding for the reprogramming factors: Klf4, cMyc, Sox2 and Oct4. Briefly, after blood collection, mononuclear cells were isolated through Ficoll (Lymphoprep) gradient centrifugation, collected and counted in a Burker chamber. PBMCs were seeded in a 24 well plate and kept in culture for 3 days in PBMC medium (Table 4). For the transduction, the reprogramming viruses were diluted in 1ml of PBMC medium. The reprogramming virus mixture was added to 5×10^5 cells previously collected in a round bottom tube and a 30 minutes centrifugation step at 1000 g was carried out to optimize the infection rate. Once the centrifugation was completed cells were seeded in a 12 well plate already containing 1 mL of fresh PMBC medium. The infection was performed with a MOI of 5 for Oct4, Sox2 and c-myc and of 3 for Klf4. The following day the Sendai viruses were removed by centrifuging the cell suspension at 200g for 10 minutes, aspirating the supernatant, and resuspending the cells in 0,5 mL complete PBMC medium. The cells were seeded again in a 24 well plate and kept in culture for 2 days. $1x10^4$-$1x10^5$ live cells were seeded in 2 mL of complete StemPro-34 (ThermoFisher) medium without the cytokines into vitronectin (ThermoFisher) coated B35 plates (Falcon). After 3 days in culture in complete StemPro-34, cells were transitioned to the iPSC growth medium, Essential 8 (ThermoFisher). Medium was daily refreshed and the growth of the first iPSC colonies was observed after one week. According to the manufacturer instructions, the live staining through TRA-1-60 antibody (ThermoFisher) was

performed to test the pluripotency of the cells and only the positive colonies were picked and transferred in a new vitronectin coated plate for amplification and further characterization.

Table 4.**iPSC reprogramming media.** List of medium composition and supplements.

PBMC medium	Complete StemPro-34	Essential 8 medium
StemPro-34 **+** **100 ng/ml SCF** **100 ng/ml FLT3** **20 ng/ml IL-3** **20 ng/ml IL-6** **2 mM L-glutamin** **+** **Company supplement**	**StemPro-34** **+** **2 mM L-glutamin** **+** **Company supplement**	**Essential 8** **+** **Company supplement**

4.1. iPSC characterization

Real Time PCR quantitative analyses (qRT-PCR) was performed assessing whether the reprogrammed iPSC were expressing the key pluripotency genes. Then, the embryoid bodies test was performed. This is a differentiation test for iPSCs that allows the expression of markers from the three different germ layers (ectoderm, mesoderm and endoderm) to be assessed and thus confirm the pluripotency of iPSCs. Briefly, iPSC were seeded in single cells in Essential 6 medium (ThermoFisher) in ultralow attachment plates (StemCell). After 7 days the presence of embryoid bodies was observed and the cells were kept in culture for 7 additional days. RNA was extracted on day 21 in order to evaluate the expression of three germinal layers markers through qRT-PCR. The following primers for endoderm, mesoderm and neuroectoderm were used and compared to the pluripotent markers (Table 5):

Table 5.**Embryoid bodies primer list.** Primers used to evaluate the expression levels of germinal layers markers comparing to the pluripotency markers in the iPSC-derived EB.

Marker for	Target	Forward 5'-3'	Reverse 5'-3'
Pluripotency	NANOG	CCATCCTTGCAAATGTCTTCTG	CTTTGGGACTGGTGGAAGAATC
	OCT4	GCAGCAGATCAGCCACATC	CTTGATCGCTTGCCCTTCT
Endoderm	AFP1	CAAAATGCGTTTCTCGTTGCT	GCTGCCATTTTTCTGGTGATG
	FOXA2	CCACCTGAAGCCGGAACA	TGCTCCGAGGACATGAGGTT
	GATA4	GCTATGCGTCTCCCGTCAG	GTGACTGTCGGCCAAGACC
Mesoderm	HAND1	AACTCAAGAAGGCGGATGG	AGGGCAGGAGGAAAACCTT
	MIXL1	GGTACCCCGACATCCACTTG	TAGCCAAAGGTTGGAAGGATTTC
Neuroectoderm	NEUROD1	GAGCACGAGGCAGACAAGAAG	CCCCCGTTCCTCAGTGAGT
	PAX6	CCGCCCTGGTTGGTATCC	TTGGTATTCTCTCCCCCTCCTT
	SOX1	ATGAAGGAGCACCCGGATTA	CTTCTTGAGCAGCGTCTTGGT

Cells karyotype was evaluated before and after the reprogramming with the aim to check whether any chromosome alteration had occurred during the reprogramming. Karyotype was analysed by staining condensed chromosomes through the G-banding technique. Briefly, cells were fixed in glacial acetic acid and methanol (1:3), they were treated with trypsin to digest histone proteins and were then put in a Giemsa solution with the aim to colour the digested rich-regions of condensed chromatin, giving as a result a specific banding pattern.

4.2. iPSC culture

iPSCs colonies were cultured in Essential 8 medium in vitronectin coated B35 plates (Falcon). For standard passaging, cells were washed once with Dulbecco's Phosphate-Buffered Saline (DPBS) without calcium or magnesium, incubated for 2 minutes at 37 °C in a solution of DPBS with 0.5 mM EDTA, this solution was aspirated, the cells were detached in 1 mL of fresh Essential 8 medium and transferred in a new vitronectin coated plate. To dissociate the iPSC colonies into single cells, the cells were washed once with DPBS and then incubated with 1 mL of accutase (ThermoFisher) for 5 minutes at 37°C. Once detached, 5mL of DMEM-F12 medium (Gibco) were added to diluted the accutase and the cells were collected in a 15 mL tube and centrifuged for 5 minutes at 300g. Cells were then resuspended in the final medium supplemented with ROCK inhibitors Y27632 10

µM (Miltenyi) according to the different protocols. KnockOut Serum (ThermoFisher) with 10 % DMSO was used to the iPSC freezing.

5. Mesoderm differentiation

iPSC were differentiated towards the mesoderm lineage with a 2D culture protocol using the STEMdiff™ Mesoderm Induction Medium (MIM) (Stem cell technologies). Briefly, $2\times10^4/cm^2$ cells were detached into single cells using accutase and were seeded in Essential 8 medium enriched with ROCK inhibitors Y27632 10 µM (Miltenyi) in a 12 well plate already coated with vitronectin. After 24 hours, the medium was replaced with STEMdiff™ MIM enriched with 2 mM of L-Glutamine and for the following 4 days, medium was changed daily. At day 4, RNA was extracted in order to assess the expression of the mesoderm markers (T, MIXL1, and NCAM) compared to the pluripotency markers OCT4, SOX2 and Nanog through quantitative Real Time PCR (qRT-PCR). Primers for mesoderm-specific expressed genes were used (Table 6).

Table 6.**Mesoderm primer list**. Primers used to evaluate the expression levels of mesoderm markers in differentiated iPSCs.

Marker for	Target	Forward 5'-3'	Reverse 5'-3'
Pluripotency	SOX2	TGCGAGCGCTGCACAT	GCAGCGTGTACTTATCCTTCTTCA
	OCT4	GCAGCAGATCAGCCACATC	CTTGATCGCTTGCCCTTCT
Mesoderm	T	GATCACAAAGAGATGATCGAGGAA	GGAAGAAGCCACCCCCATT
	NCAM	AGTGCAATATGCCCCAAAGC	TGGCACTGGGATAGGCAAAT
	MIXL1	GGTACCCCGACATCCACTTG	TAGCCAAAGGTTGGAAGGATTTC

6. Genetic and chemical inhibition of SDHA subunit

6.1. Gene editing: CRISPR/CAS9

SDHA knockout into the genome of healthy donor iPSC and SDH-deficient patient iPSC was performed. The CRISPR-Cas9 system that was used consisted in a ribonucleoprotein (RNP): a target-specific CRISPR RNA (crRNA), a transactivating crRNA (tracrRNA), and a Cas9 endonuclease (IDT-technologies). The tracrRNA has the addition of ATTO™ 550 fluorescent dye to the 5' end. A predesigned guide, able to target a region of the SDHA gene containing nucleotide

sequences not present in the SDHAP1, SDHAP2, SDHAP3 and LOC pseudogene, was chosen (Table 7) (IDT-technologies). A final concentration of 100 µM of crRNA and tracrRNA duplex was prepared through an incubation of 95 °C for 5 minute. The heteroduplexes were incubated at room temperature for 20 min with Alt-R-Cas9 Nuclease 3NLS to allow the ribonucleoprotein (RNP) complex to form. iPSC were dissociated in single cells, collected in Essential 8 medium and 1 x 10^6 were centrifuged and transfected with the RNP complex and Alt-R-Cas9 Elettroporation Enhancer mix (IDT-technologies). The stem cell Nucleofector Kit (Lonza) with the program A023 of Amaxa Nucleofector I (Lonza) was used for transfection. Cells were then plated in 10 cm coated plates in Essential 8 medium with 10 µM of ROCK inhibitors. Medium was refreshed every day and, after 1 week small colonies were picked. The efficiency of transfection was assessed through FACSCanto™ Flow Cytometer (BD) exploiting the ATTO™ 550 fluorescent dye. SDHA mutation status was assessed by Sanger sequencing on a series of 120 clones isolated by picking and subsequently expanded. Furthermore, subcloning through BD Influx flow cytometer, was performed at the Faculty of Veterinary Medicine at Utrecht University (NL), where single were cultivated in 96-well coated plates in Essential 8 medium.

Table 7.**Predesigned ALT-R-CRISPR-Cas9 gRNA (IDT-technologies**). Predesigned guide on exon 9 of SDHA gene.

Target	Position	Exon	Sequence 5'-3'	Pam
SDHA	235288	9	CCCACCGTGCATTATAACAT	GGG

6.2. DNA extraction and amplification

DNA was extracted from isolated clones using the QIAamp DNA Mini kit (Quiagen) according to the manufacturer protocol. The quantification was performed with the NanoDrop 1000 spectrophotometer (Thermo Scientific), evaluating the absorbance at 260 nm and the samples purity at 260/280 and at 260/230 ratio. QuickExtract™ DNA Extraction Solution (Lucigen) was also used for the DNA extraction. 20 ul of QuickExtract™ DNA Extraction Solution were added to the sample and after 15 seconds of vortexing, the samples were incubated at 65°C for 6 minutes. After further 15 seconds of vortexing, a final incubation at 98°C for 2 minutes was performed. 5 µL of the extracted DNA were used for PCR amplification. The primers on the exon 9 of SDHA gene sequence were designed with the Primer Express software to bind the regions with the highest number of mismatch among gene and pseudogenes (Table 8).

Table 8.**Primer pairs used for colonies screening**. Primers amplify SDHA exons and not the related pseudogenes.

Target	Exon	Forward 5'-3'	Reverse 5'-3'
SDHA	9	CACACTTCCAAGATGACGTAT	TGCGAGGTGGGCCCCGTC

FastStart Taq DNA Polymerase kit (Roche) was used for the PCR amplification. The PCR reaction mix was prepared following the manufacturer instruction, 24 ul of the mix were added to 1 µl of 10 ng/µL DNA of each sample in a final volume of 25 ul. The reaction took place in a thermocycler with the following program: 95°C for 5 min, (95°C for 30'', 69°-54° (-0.6°C /cycle) for 1', 72°C for 1') for 25 cycles; (95°C for 30'', 54°C for 1', 72°C for 1') for 10 cycles.

6.3. Sanger sequencing of isolated clones

The samples have been sequenced by Sanger procedure to check for the effective knockout of the SDHA gene. The PCR products were diluted in 70 ul of water and the whole solution was transferred into the purifying plate, the MultiScreen-PCR96 filter plate (Millipore) was connected to a vacuum pump set to 100 mbar. After 10 minutes of aspiration, 30 µl of H2O were added to the PCR products attached to the membrane of each well and vortexed. To perform Sanger Sequencing the The BigDye Terminator v1.1 Cycle Sequencing kit (Applied Biosystems) was used, following this program: 96°C for 30'', (96°C for 10'', 60°C for 4') for 25 cycles. The sequenced DNA was purified with a sodium acetate based precipitation protocol and each purified precipitate was resuspended into 10 µl of Injection Buffer (Millipore). The lecture was carried out with the 96-capillary ABI 373O DNA Analyzer (Applied Biosystems) and the Sequencher 4.1 software (Gene Codes Corporation) was used to read the electropherograms.

6.4. Chemical inhibition of SDHA subunit with 3-NPA

Healthy donor iPSCs, which were already reprogrammed and characterized were used as a control in several experiments. Healthy donor iPSCs and SDH-deficient derived iPSCs, used both before and after mesoderm differentiation, were treated with an inhibitor of SDHA FAD binding pocket of SDH subunit A, 3-nitropropionic acid (3-NPA) (Sigma). Briefly, cells were seeded into single cells, and upon reaching 80% confluency, were treated with variable concentrations (from 10 µM to 50

mM) of 3-NPA. After an incubation of 24 hours, Presto Blue® Cell Viability, LDH assay and RNA collection were performed.

6.5. Presto Blue® assay

The Presto Blue® Cell Viability (Thermofisher), resazurin based reagent was used to assess the mitochondrial activity. Presto Blue® reagent was mixed with culture medium at a 1:10 ratio. The cells were incubated at 37° C, 5% of CO2 for 1 hour with 200 ul of mix. The fluorescence was measured at excitation wavelength of 530 nm and emission wavelenght of 590 nm using the GloMax Discover Microplate Reader.

6.6. LDH Assay

Cellular cytotoxicity was assessed using the CyQUANT LDH Cytotoxicity Assay (Thermofisher). This colorimetric assay measures the release of lactate dehydrogenase (LDH) into the cell culture medium upon damage of the plasma membrane. Briefly, 50 ul of reaction mix was prepared according to the manufacturer instructions, and was added to 50 ul of supernatant. After 30 minutes of incubation at room temperature, 50 ul of Stop solution were added to the samples and the absorbance at 490 nm was measured using the a GloMax Discover Microplate Reader.

6.7. Reverse Transcription Quantitative PCR (RT-qPCR)

RT-qPCR in iPSC and differentiated samples was performed by isolating total RNA using RNeasy spin column method (Qiagen). Subsequently, 100 ug of RNA were reverse transcribed to cDNA through iScript cDNA Synthesis Kit (Biorad, The Netherlands). Following cDNA-synthesis, quantitative PCR was performed using a CFX96 Real-Time PCR detection system (Biorad, Veenendaal, The Netherlands). Specific primers for the target genes were used (Table 9). $2^{-\Delta\Delta CT}$ method was used to quantify gene expression levels normalized on three housekeeping genes: HPRT1, ATPS and YWHAZ.

Table 9.**Primer list.** Primers used to evaluate the expression levels of hypoxia and neural markers in untreated and 3-NPA treated iPSC and mesoderm cells.

Target	Forward 5'-3'	Reverse 5'-3'
HPRT1	TGCTGAGGATTTGGAAAGGGTG	ACAGAGGGCTACAATGTGATGGC
ATPS	GTCTTCACAGTTCATATGGGGA	ATGGGTCCCACCATATAGAAGG
YWHAZ	ACTTTGGTACATTGTGGCTTCAA	CCGCCAGGACAAACCAGTAT
HIF1α	TATGAGCCAGAAGAACTTTTAGGC	CACCTCTTTTGGCAAGCATCCTG
EPAS1	TTCCTGCGAACACACAAGCT	TCCAAGGCTTTCAGGTACAAGTT
LHX2	GATCTGGCGGCCTACAACG	CGAAGCTGGTGGTGCTTGAA
NEFL	CCAAGACCTCCTCAACGTGAAG	AGCTCTGGGAGTAGCCACTGG
IGF1R	TCTTCACCACTTACTCGGACGTCT	GGTTATACTGCCAGCACATGCG
CDH2	GTGGACAGGATTGTGGGTGC	CGTTCTTTATCCCGGCGTTT

RESULTS

1. Molecular and clinical analysis of SDHA-deficient GISTs

1.1. Germline mutational analysis

The aim of this part of the study was to uncover the prevalence of germline SDHA mutation in GIST patients carrying an SDHA mutant tumor, to clarify the contribution of an heritable tumor-predisposing mutation to SDHA-deficient GIST onset. Sanger sequencing of 14 samples was performed to evaluate the presence of SDHA variants in the germline lineage in an SDH-deficient GIST series carrying SDHA somatic mutations. The presence of germline mutations was found in all 14 patients for which the normal counterpart was available (Table 2). Specifically, five truncating nonsense variants (Ser384*, Arg31*, Trp119*, Arg210*), seven missense variants (Gly233Val, Arg171His, Arg589Gln, Gly257Ala, Arg600Gln, Arg585Gln) and two exon-flanking intronic variants predicted to affect splicing were found in our population. Both splice site alterations, as predicted, lead to a stop codon formation. Following the ACMG recommendations we categorised all the nonsense mutations, one splice-site and two missense mutations as “Pathogenic” or “Likely Pathogenic” and the other five mutations as “Uncertain Significance” (Table 10). The computational prediction algorithms implemented in Varsome classified the variant with "Uncertain Significance" as damaging. With regards to the mutational status of the tumour, eight tumour DNA, showed homozygosity for the germline variant due to the loss of the corresponding wild-type allele; in the other six cases an additional somatic mutation was observed, thus resulting in compound heterozygosity (Arg589Trp, Arg451Cys, Arg171Cys, Arg585Gln, Thr308Met and Gln176*) (Figure 3A). Tumour DNA from patients whose normal counterpart was not available carried two mutational hits on the SDHA gene. In accordance with other studies, the germline SDHA variants are scattered along the whole coding sequence (Figure 3B). The truncating Arg31* variant is the one most frequent identified in literature and was found in one case in our series[22,42,44-74, 67-70].

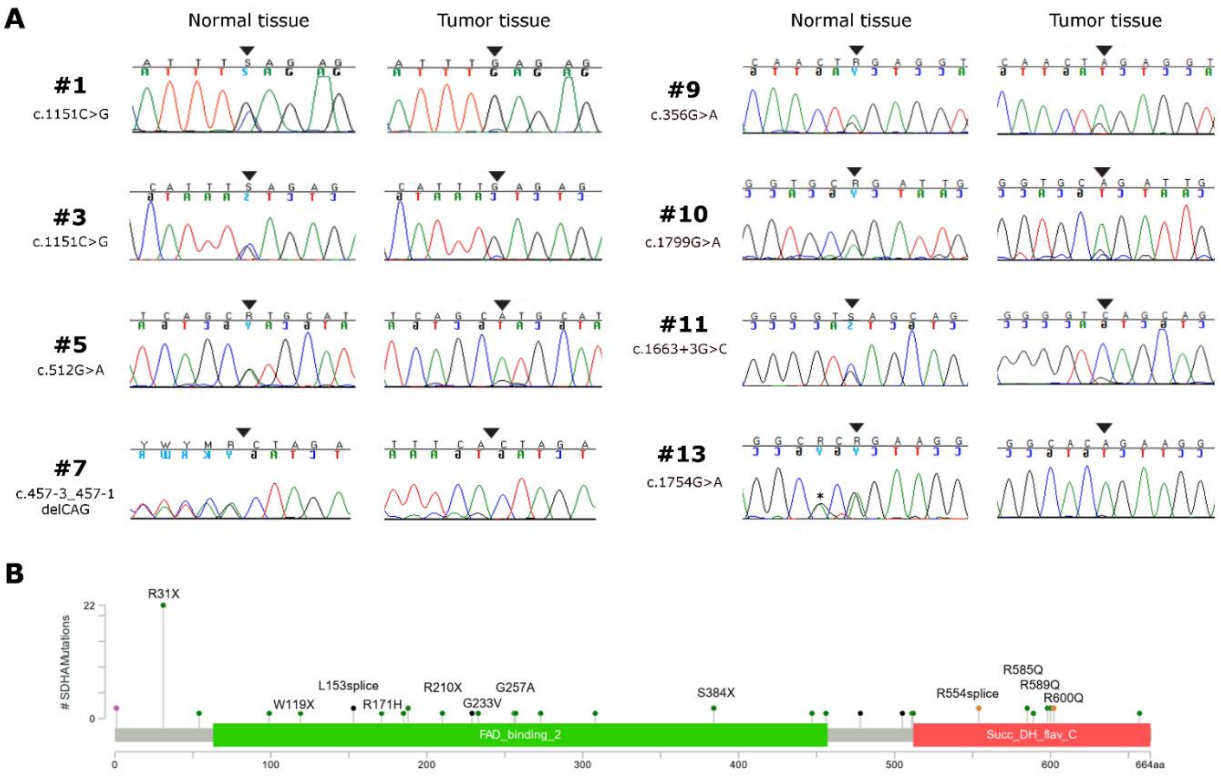

Figure 3.A) **Chromatograms indicating the loss of heterozygosity of SDHA germline variants in tumor tissue of eight SDH-deficient GIST patients.** The position of the mutation is indicated with the black arrows; the asterisk indicates a silent single nucleotide polymorphism. B) SDHA germline variant frequency of GIST patients of our series (written protein mutation) and of previous studies[23,43,46,49,69,47,70,48,71, ,72,] shown as lollipop plot.

Table 10.**Mutational analysis of germline and tumours in SDHA-deficient GIST patients.** The cDNA and protein mutation in the normal germline and the second somatic mutation in GIST is reported, along with the variant classification following ACMG recommendations, the allelic status and the allelic frequency in the general population (gnomAD database). PB, peripheral blood; FF, fresh-frozen; NA, not available, ND, not detected; P, pathogenic; LP, likely pathogenic; UNC, uncertain significance.

Pts N°	Normal counterpart germline variant						Tumor Tissue somatic mutation			
	Sample	Mutation	Variant classification	Exon	Status	gnomAD Frequency	Sample	Mutation	Variant classification	Exon
#1	PB	c.1151 C>G; p.Ser384*	P	9	Hetero	$7.96x10^{-6}$	FF	LOH	P	9
#2	PB	c.91 C>T; p.Arg31*	P	2	Hetero	$2.09x10^{-4}$	FF	c.1765 C>T; p.Arg589Trp	LP	13
#3	PB	c.1151 C>G; p.Ser384*	P	9	Hetero	$7.96x10^{-6}$	FF/ FFPE	LOH	P	9
#4	PB	c.698 G>T; p.Gly233Val	UNC	6	Hetero	ND	FFPE	c.1351 C>T; p.Arg451Cys	UNC	10
#5	PB	c.512 G>A; p.Arg171His	UNC	5	Hetero	$1.41x10^{-5}$	FFPE	LOH	UNC	5
#6	PB	c.1766 G>A; p.ArgR589Gln	LP	13	Hetero	ND	FF	c.511C>T; p.Arg171Cys	UNC	5
#7	PB	c.457-3_457-1 delCAG; p.L153splice	P	5	Hetero	ND	FFPE	LOH	P	5
#8	PB	c.770 G>C; p.Gly257Ala	P	6	Hetero	ND	FFPE	c.1754G>A; p.Arg585Gln	UNC	13
#9	FFPE	c.356 G>A; p.Trp119*	P	4	Hetero	ND	FF	LOH	P	4
#10	FFPE	c.1799 G>A; p.Arg600Gln	UNC	14	Hetero	$2.09x10^{-5}$	FFPE	LOH	UNC	14
#11	PB	c.1663+3 G>C; p.R554splice	UNC	12	Hetero	$1.59x10^{-5}$	FFPE	LOH	UNC	12
#12	FFPE	c.1799 G>A; p.Arg600Gln	UNC	14	Hetero	$2.09x10^{-5}$	FFPE	c.923C>T; p.Thr308Met	UNC	8
#13	FFPE	c.1754 G>A; p.Arg585Gln	UNC	13	Hetero	$7.97x10^{-6}$	FFPE	LOH	UNC	13
#14	FFPE	c.628 C>T; p.Arg210*	P	6	Hetero	$3.98x10^{-6}$	FFPE	c.526C>T; p.Gln176*	P	5
#15	NA	NA	NA	NA	NA	NA	FFPE	c.923C>T; p.Thr308Met c.1741G>A; p.Gly581Arg	UNC+ LP	8+13
#16	NA	NA	NA	NA	NA	NA	FFPE	c.1255 G>A; p.Gly419Arg c.1690 G>A; p.Glu564Lys	UNC+ UNC	9+13

1.2. Clinical findings

Regarding the clinical results, the patient's average age at diagnosis was 39.5 ± 4.5 years (range 17-70). Specifically, in our series, ten cases were young-adults (range: 17-39 years old) and 6 patients were older-adults (> 50 years old; range: 50-70). According to the literature[22,42,44,74,67-70], we can assert that GISTs arise at very different age ranges in SDHA-variant carriers (mean age at diagnosis is 36.0 ± 2.3 years), but up to 22% of patients are being diagnosed at more than 50 years old (Figure 4). Through this study, we confirmed that the stomach is the unique localization of GIST onset but highlights a higher heterogeneity for the multifocality development and also for the metastatic presentation at diagnosis. Specifically, in all cases of adult patients, the GIST was unifocal. In the whole series the GIST was localized, however four patients showed metastases already at the time of diagnosis. In all cases GIST was the only disease presentation, and no personal or familial cancer history was revealed, except for one case of 61 years of age at diagnosis that was affected by paraganglioma more than 10 years before. Unfortunately the biological material was not available for further tests. Except for two cases lost at follow up, the mean follow-up time was 10.9 years, (range: 2.2 - 22.8 years). Three of the localized cases developed a recurrence with multiple metastases. Overall, seven metastatic cases have been treated with standard medical therapy

integrated with surgery and/or others loco-regional therapy (radiofrequency of liver metastasis and also chemoembolization in one case). Among these 7 metastatic cases, one is currently free of disease as a result of the complete surgical removal of liver metastases and one died of the disease.

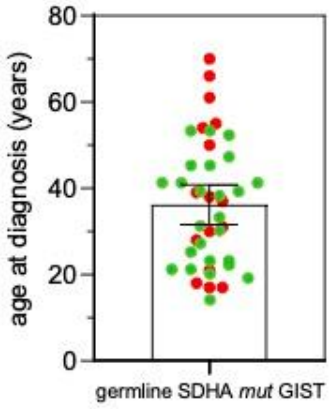

Figure 4.**Age at GIST onset in SDHA-variant carriers.** The mean and SEM are shown. Red, patients from our series; Green, patients from previously published reports[22,42,44-74, 67-70].

2. Gene expression profile of SDH-deficient GIST

2.1. Gene expression analysis

The aim of this part of the project was to investigate and discover signalling pathways that could be potential therapeutic targets. Gene expression analysis was performed separately for fresh frozen tissue and FFPE samples, which were analysed with microarray and RNA-seq respectively. Firstly, an unsupervised analysis, by using PCA, was performed in order to decompose the transcriptome data variability into three-dimensional components. The 3D projections revealed that SDH-deficient GISTs have an expression profile extremely different from KIT-mutant GISTs, indeed both PCA analysis showed the separation along the second component between SDH-deficient GISTs and KIT-mutant GISTs. These results support the hypothesis of a different cell types derivation between the two GIST molecular subgroups (Figure 5A,B).

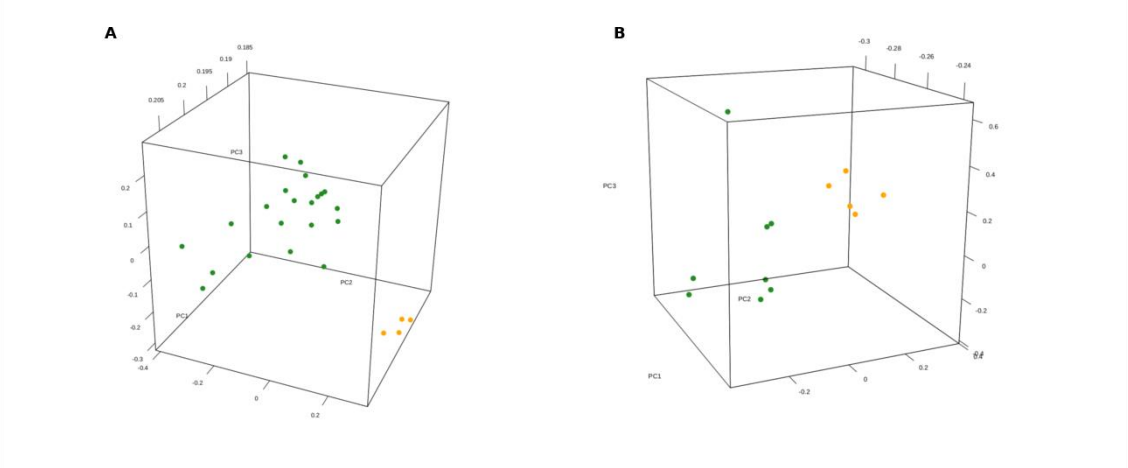

Figure 5.**Principal component analyses (PCA**). A) PCA was performed on samples analysed with microarray (number of SDH deficient GISTs = 4; number of KIT-mutant GISTs = 21). B) PCA performed on samples analysed with RNA-seq (number SDH-deficient GISTs = 5; number of KIT-mutant GISTs = 8). The analysis shows that SDH-deficient GISTs (orange points) distinctly separate from KIT-mutant GISTs (green points).

Subsequently, the analysis of DE was performed for both sample series to study the set of genes that are significantly overexpressed or down-regulated in SDH-deficient GISTs. For fresh frozen samples, 833 and 928 genes were found respectively up- and down-regulated (adjusted p-value < 0.05); for the FFPE samples, 577 genes were overexpressed and 889 genes were underexpressed (adjusted p-value < 0.05). Then, the data were intersected to identify the over/under expressed genes commonly modulated in the two series of samples, highlighting 405 overexpressed and 331 under expressed genes in SDH-deficient GISTs. These two sets of genes were used to perform the over-representation analysis with the Enrich web tool. The significantly over-represented pathways (adjusted p-value < 0.05) for up- and downregulated genes are described in Tables 11 and 12. The set of genes upregulated in the SDH-deficient group are relate to hedgehog signalling, hypoxia, glycolysis, and epithelial-to-mesenchymal transition (EMT). On the contrary, among the down-regulated pathways, we discovered immune system related pathways, such as interferon gamma/alpha response, IL/STAT signalling, TNF-alpha signalling, and complement; in addition, fat metabolism and KRAS signalling were also highlighted.

Table 11.Over-representation analysis by MSigDB.

Database	Terms	p-value
MSigDB Hallmark up-regulated genes	Hedgehog Signaling	0,000010
	Hypoxia	0,0026
	UV Response Dn	0,0027
	Estrogen Response Early	0,0078
	Glycolysis	0,0078
	Apical Junction	0,021
	Epithelial Mesenchymal Transition	0,021
MSigDB Hallmark down-regulated genes	TNF-alpha Signaling via NF-kB	0,000010
	Interferon Gamma Response	0,00013
	KRAS Signaling Up	0,00013
	Fatty Acid Metabolism	0,00031
	IL-2/STAT5 Signaling	0,00050
	Complement	0,0019
	IL-6/JAK/STAT3 Signaling	0,0032
	Bile Acid Metabolism	0,011
	Adipogenesis	0,019
	Interferon Alpha Response	0,023

Interestingly, also the cell type over-representation analysis of up-regulated genes showed significant genes linked to neuronal and brain tissues such as Fetal brain, pineal gland, prefrontal cortex, and superior cervical ganglion (Table 12), while among the list of down-regulated genes we found cell types mainly related to hematopoietic lineage, such as CD33+ myeloid, CD14+ monocytes, and CD56+ natural killer (NK) Cells.

Table 12.Over-representation analysis by Human Gene Atlas.

Database	Terms	p-value
Human Gene Atlas up-regulated genes	Fetalbrain	0
	pineal night	0,000010
	PrefrontalCortex	0,00043
	Amygdala	0,00072
	pineal day	0,0041
	SuperiorCervicalGanglion	0,011
	Thyroid	0,013
	CerebellumPeduncles	0,022
	BronchialEpithelialCells	0,028
Human Gene Atlas down-regulated genes	CD33+ Myeloid	0,00018
	CD14+ Monocytes	0,00069
	CD56+ NKCells	0,0017
	Prostate	0,0030
	Liver	0,015
	BronchialEpithelialCells	0,019
	Adipocyte	0,031

Subsequently, the whole expression matrices (form both microarray and RNA-seq analysis) was used to run the GSEA tool. The aim of this analysis was to further investigate the presence of enriched and depleted pathways in SDH-deficient GISTs. Furthermore, the results given by RNA-seq and microarray data were intersected to highlight the strongest and clearest signals. Based on our data, SDH-deficient GISTs share three significant pathways: the fibroblast growth factor receptor (FGFR) signalling, the glycosamminoglicane (GAG) degradation and VXPX CARGO TARGETING TO CILIUM (the process of driving membrane proteins containing the motif valine-X-proline-X in the C-terminal tail towards the ciliary membrane) (Table 13). On the other hand, among the commonly depleted pathways we found the immune system related such as the cascade of Toll-like receptor complex, the IL3 pathway, the high-affinity IgE receptor signalling, and the granulocyte macrophage colony-stimulating factor. These results made us assume that SDH-deficient GISTs are characterized by the activation of several gene signatures related to invasion and tumour progression, and are also marked by the depletion of immune competence. Thus, we focused our investigation in neural like signatures, FGFR signalling, hypoxia, EMT, and immune-related signatures.

Table 13.**Gene Set Enrichment analysis (GSEA).**Significantly enriched pathways highlighted in both microarray and RNA-seq series.

	Microarray		RNA-seq	
Pathway name	**NES**	**p-value**	**NES**	**p-value**
REACTOME PHOSPHOLIPASE C MEDIATED CASCADE FGFR2	1.802	0.022	1.354	0
REACTOME_FGFR2_LIGAND_BINDING_AND_ACTIVATION*	1.717	0.044	1.313	0.062
WP GLYCOSAMINOGLYCAN DEGRADATION	1.686	0.041	1.346	0.025
REACTOME VXPX CARGO TARGETING TO CILIUM	1.576	0.019	1.276	0.040

2.2. Overexpression of Neural Markers

Our pathway analysis highlighted that SDH-deficient GISTs are characterized by the overexpression of a significant number of genes related to the commitment to neural lineage. In particular, this analysis confirmed the overexpression of genes previously described such as the transcriptional regulator LHX2 (known to be associated with the neural crest differentiation), the neurofilament

light polypeptide NEFL, the synaptic cell adhesion molecule belonging to the nephrin-like family KIRREL3, the N-cadherin CDH2, and the neural progenitor-specific gene IGF1R[73]. Moreover, the overexpression of further important neural marker such as the glutamate receptor GRIA1, the integrin-8 ITGA8, and the neuronal cell adhesion molecule NRCAM was also observed. This scenario suggests that SDH-deficient GISTs might derive from a different cell type (with respect to the more common GIST molecular subtype) and in particular, from cells committed to neural differentiation. It is already known that GISTs originate from mesenchymal cells, namely, interstitial cells of Cajal (ICC), located within the gastrointestinal tract and involved in the crosstalk between smooth muscle and nervous system. We discovered that the majority of ICC markers were highly and equally expressed in both GIST subgroups; however, we found that genes linked to the induction and inhibition of neural differentiation are differential expressed. THBS4 and ELOVL6 resulted more expressed in SDH-deficient GISTs, as well as EDN3 and GJA1 were under-expressed in SDH-deficient GISTs group.

2.3. Fibroblast Growth Factor Receptor 2 Binding and Activation

Among the top up-regulated pathways, the enrichment analysis detected those related to fibroblast growth factors (FGFs) activation and the corresponding receptors (FGFRs) cascade. Even if FGFR genes were equally modulated in both groups, FGFR1 and FGFR2 showed a high expression level in all samples, while FGFR3 and FGFR4 were less expressed. On the contrary, a large set of FGF ligands (FGF4, FGF2, FGF7, and FGF10) and cell adhesion molecules (NRCAM and NCAM2) were strongly expressed in the SDH-deficient group (Figure 6). It is already known that the NCAMs–FGFRs interaction promotes the FGFRs stabilization and recycling to the cell surface of the receptors, indicating that FGFRs are activated by NCAMs in a very different way with respect to FGFs[74]. The concomitant presence of an increased level of both FGFs and NCAMs suggested that in SDH-deficient GISTs there are two different conditions that possibly lead to FGFRs activation.

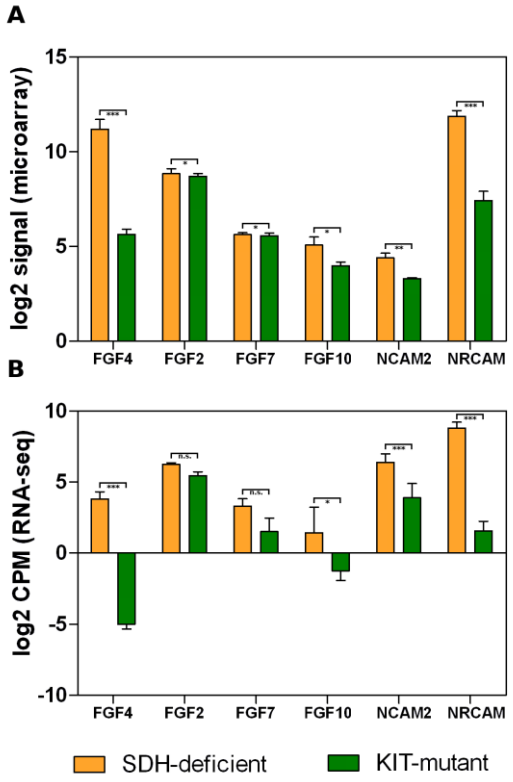

Figure 6.**Box plots showing differences in expression levels of FGFs and NCAMs for the microarray series.** (A) and RNA-seq series(B). Orange boxes represent SDH-deficient GISTs; green boxes represent KIT-mutant GISTs. Significance level: *** p-value < 0.001; ** 0.001 ≤ p-value < 0.01; * 0.01 ≤ p-value < 0.05; n.s., not significant.

2.4. Comparison with SDH-Deficient Pheochromocytoma and Paraganglioma

Our microarray GIST series and a set of SDH-deficient pheochromocytoma and paraganglioma analysed with the same protocol Affymetrix HG-U133 Plus 2.0 (available at E-MTAB-733 ArrayExpress) were also compared. The aim of this comparison was to evaluate whether the expression profile and gene signatures were related to the loss of function of SDH complex, a shared feature of these two tumours. As a first step, the whole expression profiles of SDHB-mutant pheochromocytoma/paraganglioma and our microarray GIST samples (both SDH-deficient and KIT-mutant) was compared in an unsupervised analysis by using PCA. The 3D projections showed the GIST distinctly separated from pheochromocytoma/paraganglioma (Figure 7A). This result clearly suggests that the global gene expression specifically separates the two cancer types, probably due to the different histological derivations driving the transcriptional profile. Then, we focused on

specific signature enriched in our SDH-deficient GISTs, the EMT pathway. The acquisition of mesenchymal type from epithelial cells, referred to as EMT, is normally associated to the embryonic development or to the tissue regeneration in adults. Moreover, EMT may occur during the tumor progression, inducing metastatic activity and increasing malignancy[75]. Several genes linked to EMT signature are overexpressed in our SDH-deficient GISTs such as cadherins CDH2 and CDH6, the cytokine receptor CRLF1, the secretory protein SCG2, the amyloid precursor APLP1, the enolase ENO2, and the secreted protein MGP. By selecting this set of genes, a cluster analysis was performed. SDH-deficient GISTs and pheochromocytoma/paraganglioma were distinctly separate from KIT-mutant GISTs (Figure 7B). This observation suggests that the EMT expression pattern is a shared feature among tumors with deficit of SDH complex. In addition, we found the overexpression of the basic helix-loop-helix transcription factor, TWIST1, that is known to be associated to the EMT process and to play an important role in embryonic development, suggesting the existence of a diverse grade of differentiation that is shifted towards an early stage. Finally, following the same procedure, the hierarchical clustering was performed for the hedgehog signalling and hypoxia pathways. Particularly, SDH-deficient GISTs revealed the up-regulation of hedgehog signaling, we found that GISTs and pheochromocytoma/paraganglioma are clustered together and are both separated from KIT-mutant GISTs (Figure 7C). Moreover, the cluster analysis showed that SDH-deficient GISTs and SDHB mutant pheochromocytoma/paraganglioma shared the expression of hypoxia genes (FOXO3, VLDLR, and ENO2) (Figure 7D). The hypoxia condition was associated with the overexpression of genes encoding for glutamate receptors[76], and in our data, as a matter of fact, we found the glutamate receptor GRIA1 to be one of the most up-regulated genes in SDH-deficient GISTs in both RNA-seq and microarray datasets.

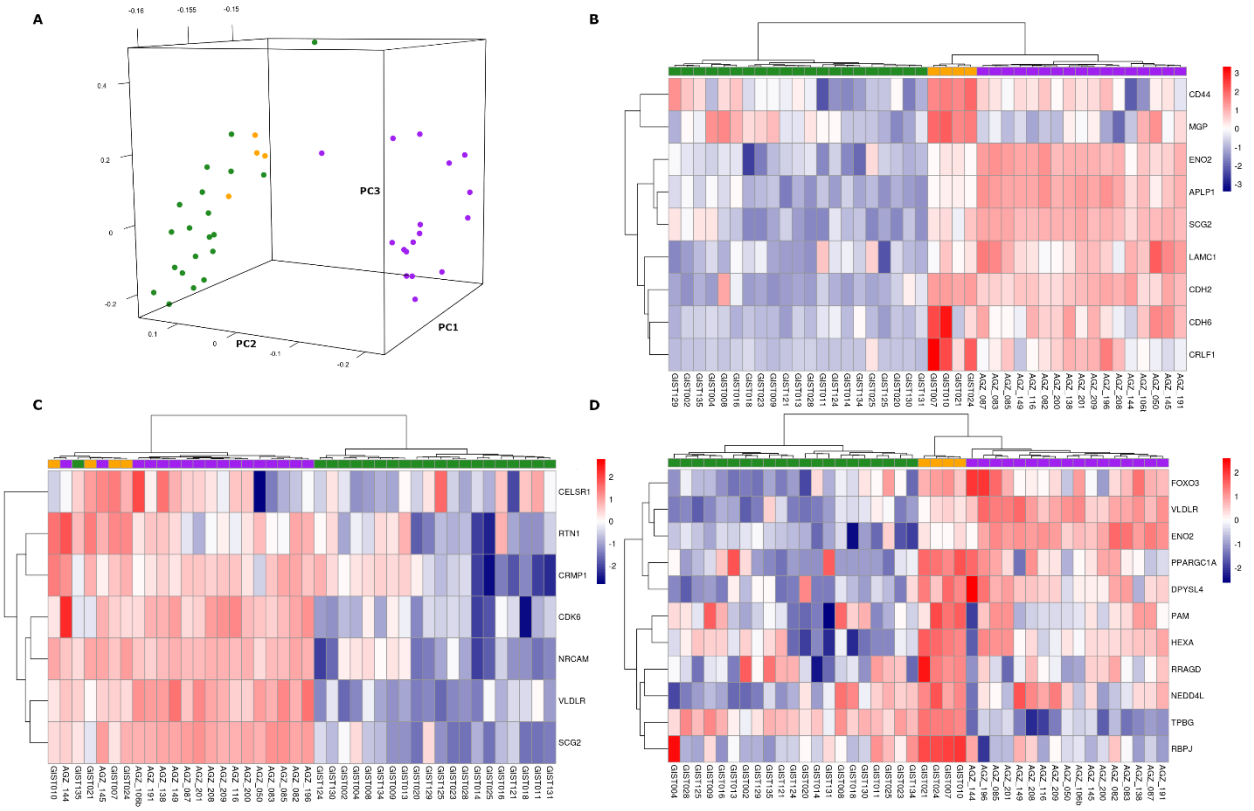

Figure 7.**Comparative analysis between GISTs analyzed with microarray (number of SDH-deficient GISTs = 4; number of KIT-mutant GISTs = 21) and pheochromocytoma/paraganglioma carrying succinate dehydrogenase complex subunit B (SDHB) mutations.** PCA highlights that GISTs (both SDH-deficient and KIT-mutant) cluster separately from pheochromocytoma/paraganglioma (A). Hierarchical clustering for the sets of genes emerged by enrichment analysis for the signalling of epithelial-to-mesenchymal transition (EMT) (B), hedgehog pathway (C), and hypoxia (D). Colour labels orange, green, and purple correspond respectively to SDH-deficient GISTs, KIT-mutant GISTs, and pheochromocytoma/paraganglioma samples.

Summing up, the gene expression analysis showed that SDH-deficient GISTs are characterized by the activation of several gene signatures linked to invasion and tumor progression. Specifically, neural like signatures, FGFR signaling, hypoxia, EMT appeared distinctive of SDH deficient GIST. The depletion of immune competence in SDH-deficient GIST was also observed.

2.5. SDH-Deficient GIST Immune Profiling

CIBERSORT analysis was performed separately for microarray and RNA-seq data to comparatively evaluate the tumor microenvironment composition in the two GIST molecular subgroups. The analysis showed that M2 macrophages and the CD4+ T-cell memory resting are the more abundant cell types in both GIST groups (Figure 8A-B). These results are in agreement with previously performed studies[68,77]. Overall, neither relative nor absolute abundance of tumor microenvironment

subpopulations allowed us to cluster SDH-deficient GISTs separately from KIT-mutant GISTs; however, the t-test analysis at single subpopulation level illustrated some remarkable evidences. In particular, SDH-deficient GISTs exhibited a significantly lower abundance of M1 macrophages (p-value = 0.03) and NK cells (p-value < 0.01) in microarray data, and similar trends were found in RNA-seq data (Figure 8C–F). Moreover, SDH-deficient GISTs in RNA-seq samples showed a statistically significant lower level of CD8+ T-cells (p-value < 0.01) and dendritic cells (p-value = 0.03), which was also confirmed in the microarray series without reaching significance (Figure 8G–J).

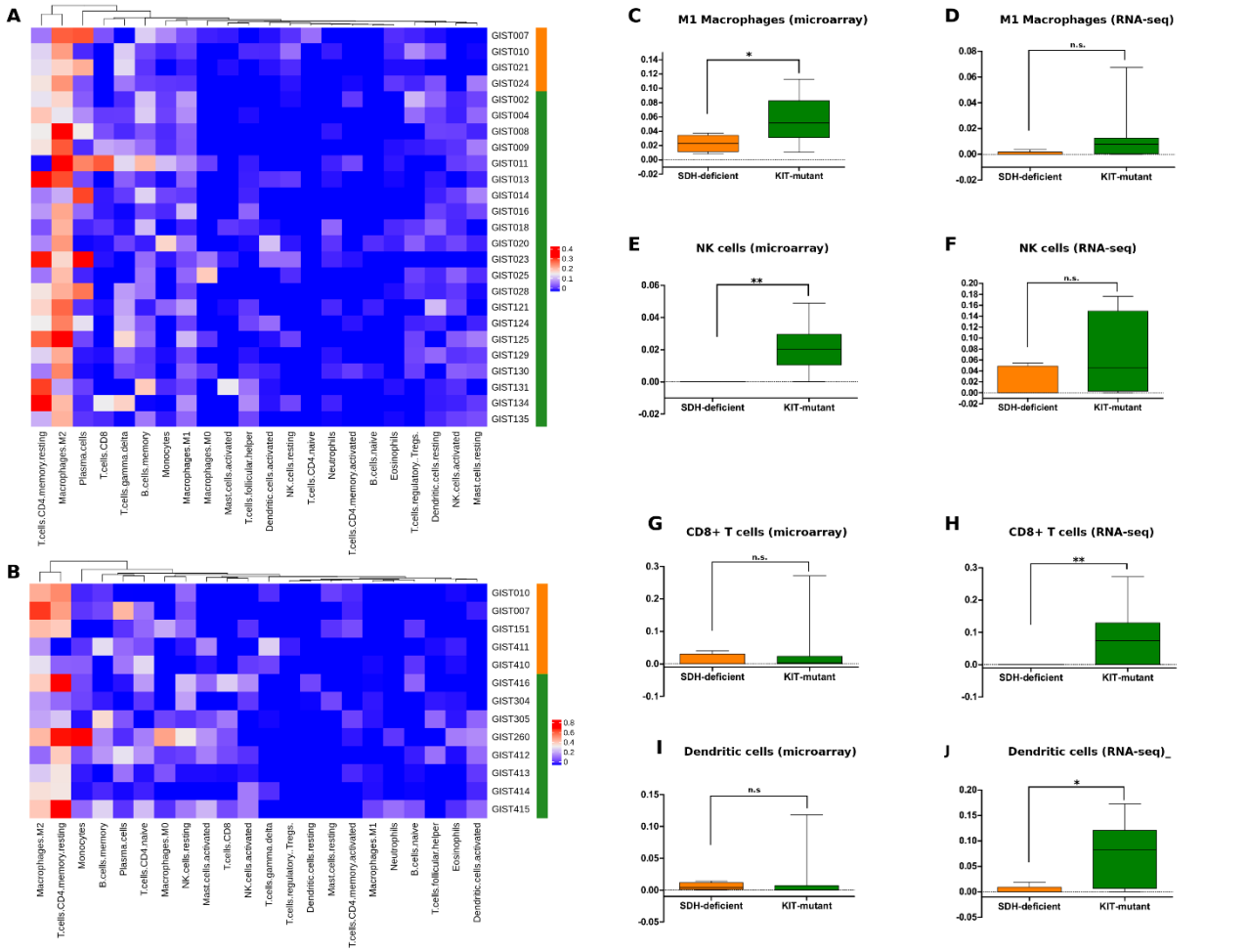

Figure 8.**Tumor microenvironment analysis by CIBERSORT**. Heatmaps represent the abundance of tumor-infiltrating cell subpopulations detected by microarray ((A) number of SDH-deficient GISTs = 4; number of KIT-mutant GISTs = 21) and RNA-seq ((B) number of SDH-deficient GISTs = 5; number of KIT-mutant GISTs = 8). Box plots (C–J) show the significant differences in the two GIST molecular subgroups of M1 macrophages, NK cells, CD8+ T-cells, and dendritic cells. Significance level is expressed as follow: ** p-value < 0.01; * 0.01 < p-value < 0.05; n.s., not significant. Orange labels correspond to SDH-deficient GISTs, while green labels correspond to KIT-mutant GISTs.

Moreover, immune-related gene signatures, the expanded IFN-induced immune signature (EIIS) and the T-cell-inflamed signature (TIS), were also evaluated. We observed that the EIIS score is lower in SDH-deficient GISTs (Figure 9).

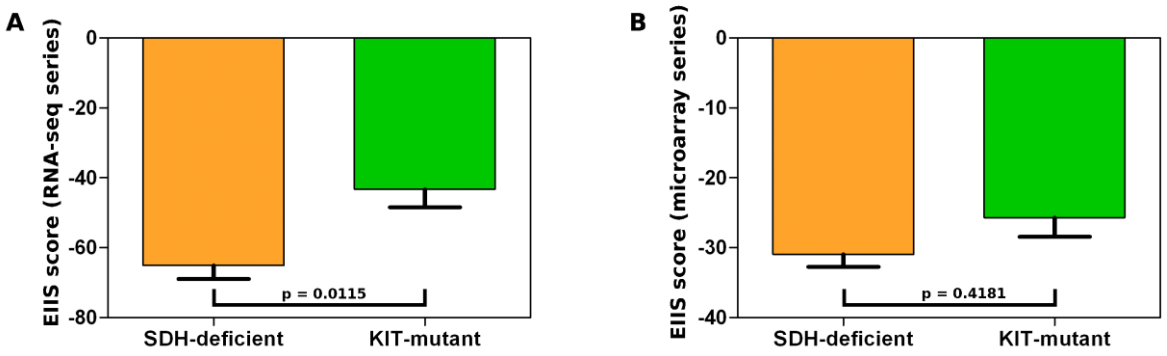

Figure 9.**IFN-γ-induced immune signature (EIIS) score in SDH-deficient GISTs (orange box) and KIT-mutant GISTs (green box)** computed for the microarray series (A) and for the RNA-seq samples (B).

Finally, TIS score were evaluated, comparing the results with the TIS score distribution in tumor types collected in The Cancer Genome Atlas (TCGA) database. Interestingly, SDH-deficient GISTs showed TIS scores closer to glioblastoma multiforme and kidney renal papillary cell carcinoma, while KIT-mutant GISTs were placed near to breast cancer and pancreatic adenocarcinoma. We included in this analysis also the GISTs of our previous series[68], excluding the KIT-mutant GISTs and keeping the PDGFRA mutant GISTs. In strong agreement with our previous findings[78], PDGFRA-mutant GISTs are confirmed as the most immunogenic GIST molecular subgroup, showing a TIS score very similar to that of tumor types known to benefit from immunotherapy (such as lung cancer) (Figure 10). On the contrary, the TIS data obtained for SDH-deficient GISTs, paired to a lower EIIS expression and to the tumor immune microenvironment depletion, suggested that this GIST subgroup should be considered as a non-inflamed tumor for which immunotherapeutic approaches could be inefficacious.

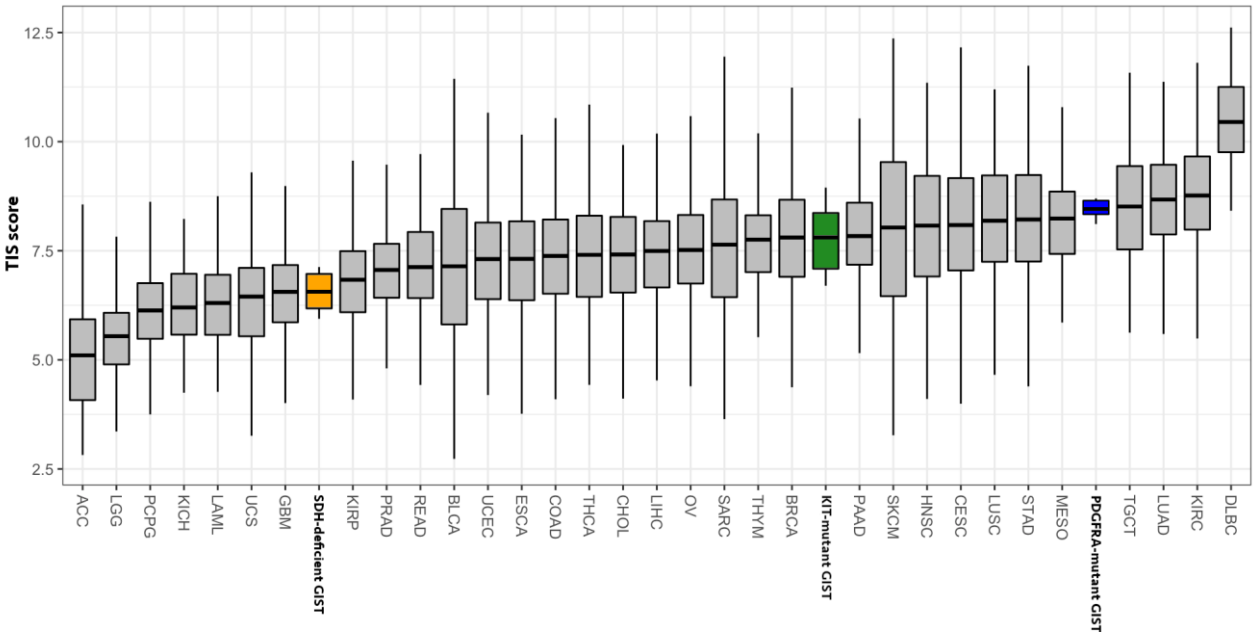

Figure 10.**T-cell-inflamed signature score of GISTs (SDH-deficient GISTs in orange, KIT-mutant GISTs in green, and PDGFRAα mutant GISTs in blue) and other solid tumor types from The Cancer Genome Atlas (TCGA)**. ACC: adrenocortical carcinoma; BLCA: bladder urothelial carcinoma; BRCA: breast invasive carcinoma; CESC: cervical squamous cell carcinoma and endocervical adenocarcinoma; CHOL: cholangiocarcinoma; COAD: colon adenocarcinoma; DLBC: lymphoid neoplasm diffuse large B-cell lymphoma; ESCA: esophageal carcinoma, GBM: glioblastoma multiforme; HNSC: head and neck squamous cell carcinoma; KICH: kidney chromophobe; KIRC: kidney renal clear cell carcinoma; KIRP: kidney renal papillary cell carcinoma; LAML: acute myeloid leukemia; LGG: brain lower-grade glioma; LIHC: liver hepatocellular carcinoma; LUAD: lung adenocarcinoma; LUSC: lung squamous cell carcinoma, MESO: mesothelioma; OV: ovarian serous cystadenocarcinoma; PAAD: pancreatic adenocarcinoma; PCPG: pheochromocytoma and paraganglioma; PRAD: prostate adenocarcinoma; READ: rectum adenocarcinoma; SARC: sarcoma; SKCM: skin cutaneous melanoma; STAD: stomach adenocarcinoma; TGCT: testicular germ cell tumors; THCA: thyroid carcinoma; THYM: thymoma; UCEC: uterine corpus endometrial carcinoma; UCS: uterine carcinosarcoma; UVM: uveal melanoma.

3. Generation of iPSC from SDHA-deficient patient

This final part of the project aimed to develop a cell model by using iPSCs to reproduce a disease model in vitro that could be used for pharmacological testing. The patient enrolled in the study carries a germline mutation c.1766 G>A, R589Q, in heterozygosity, at the level of exon 13 of SDHA. The patient has then developed in the tumour the somatic mutation c.511C>T, p.R171C, in heterozygosity, at the level of exon 5 of SDHA subunit. To generate human iPSCs from the SDHA-deficient patient, PBMCs were isolated and reprogrammed through the infection of the reprogramming factors using Sendai virus vector (Figure 11A). Two weeks after the infection of the colonies, the typical iPSC-like morphology was observed in the cultures. As a first step, a live staining with TRA 1-60 conjugated antibody was performed to demonstrate the pluripotent state of the colonies (Figure 11B). According to the morphological features and positive TRA-1-60 staining, the colonies were picked and expanded in iPSC medium for molecular characterization. After verifying the loss of the viral genome, quantitative-PCR analyses showed a high expression of the endogenous pluripotency factors SOX2 and OCT4 in the picked colonies (Figure 11C). Moreover, karyotype analysis was performed to confirm the maintenance of the normal karyotype before and after the reprogramming process. Both PBMCs and iPSCs had normal diploid 46, XX karyotype, without acquired detectable abnormalities after reprogramming (Figure 11D).

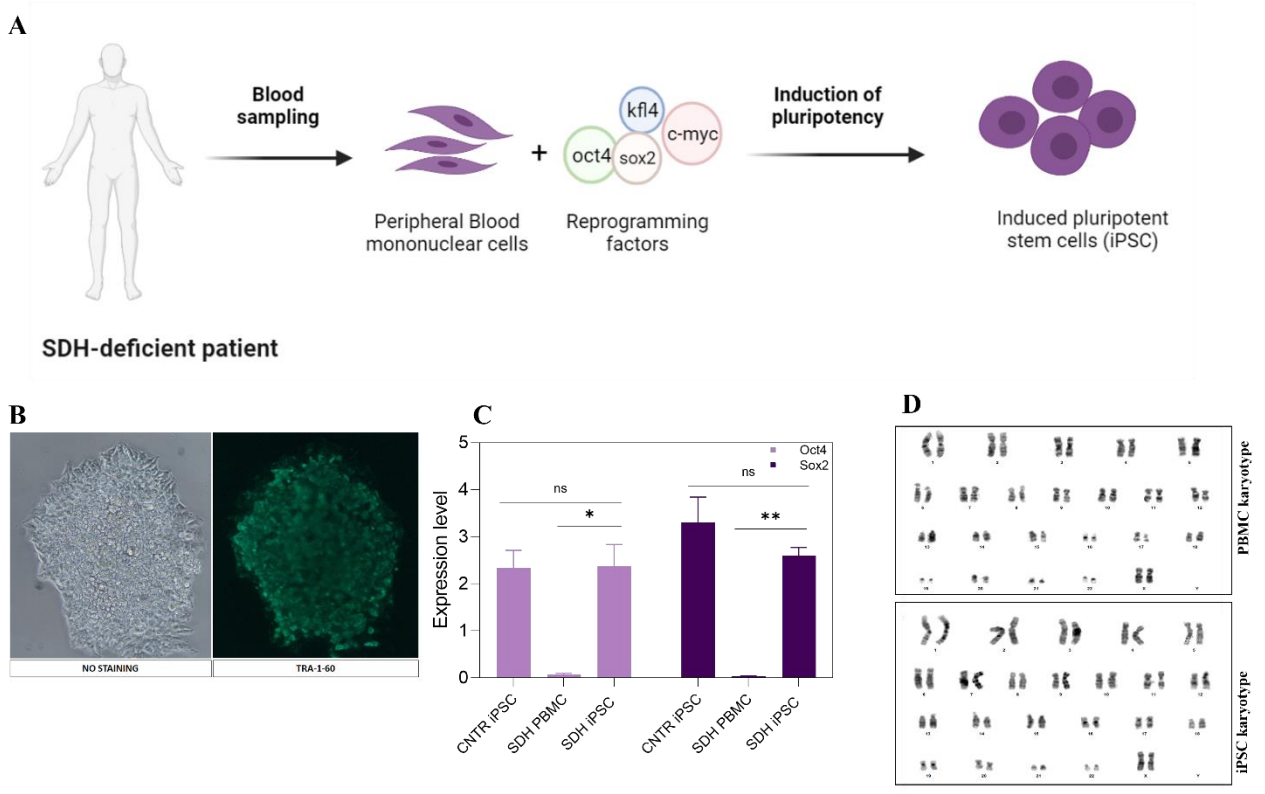

Figure 11.**SDHA iPSCs characterization.** A) Schematic representation of reprogramming process. B) TRA-1-60 positive colony (green) of SDHA patient derived iPSC. C) Expression levels of the pluripotent markers evaluated through quantitative PCR (qPCR) after reprogramming of PBMCs; iPSCs show a higher level of pluripotency markers, Sox2 and Oct4, compared to PMBC. Already characterized healthy donor iPSC lines were used as a control (CNTR iPSC). Statistical significance is indicated as p-value (Welch's test), *p=0,02, **p=0,005; ns: not significant. Each bar represents the mean value ± SEM.. D)Normal karyotype before and after reprogramming process.

Furthermore, the ability of iPSCs to spontaneously differentiate into embryoid body (EB) was evaluated through the differentiation in low attachment culture condition (Figure 12A). After three weeks, qPCR was performed to evaluate the expression levels of pluripotency and germinal layers markers. qPCR data showed a strong decrease in the pluripotency markers levels when compared to the iPSC state, while the expression level of all tri-lineage markers (mesoderm, endoderm and neuroectoderm) were considerably increased (Figure 12B).

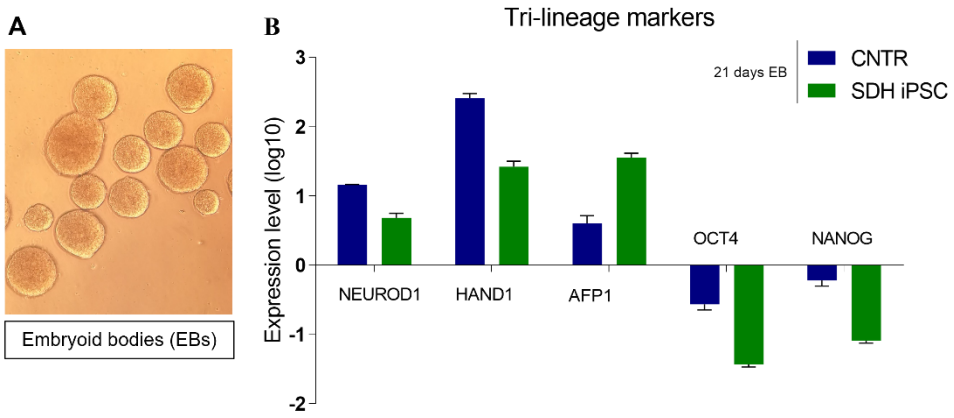

Figure 12.**Evaluation of embryoid bodies (Ebs)**. A)The image shows the embryoid bodies obtained by suspension differentiation. B) qPCR analysis of spontaneous differentiation using markers of pluripotency (OCT4 and NANOG), and the three germ layers embryonic [ectoderm (NEUROD1), mesoderm (HAND1), and endoderm (AFP1)]. The expression level of all the analysed germ lineage markers increases in the embryoid body state. On the contrary, pluripotency markers levels decrease in both populations.

3.1. Differentiation towards mesoderm

Considering the mesenchymal origin of GISTs, mesoderm differentiation was carried to try to better understand the molecular basis of this tumour and to obtain a more physiologically relevant model of the disease. Specifically, SDH-deficient derived iPSCs, together with the CNTR lines, have been differentiated towards the mesoderm lineage (Figure 13A). No differences were observed between the control line and the SDH-deficient derived iPSCs, thus only the data from SDH-deficient derived iPSCs are shown. Briefly, colonies of both iPSC lines were cultured in mesoderm induction medium for 5 days. Q-PCR analysis at day 4 demonstrated an up-regulation in the early mesoderm genes (T, MIXL1, and NCAM) and a down-regulation in iPSC markers (Nanog and SOX2) (Figure 13B).

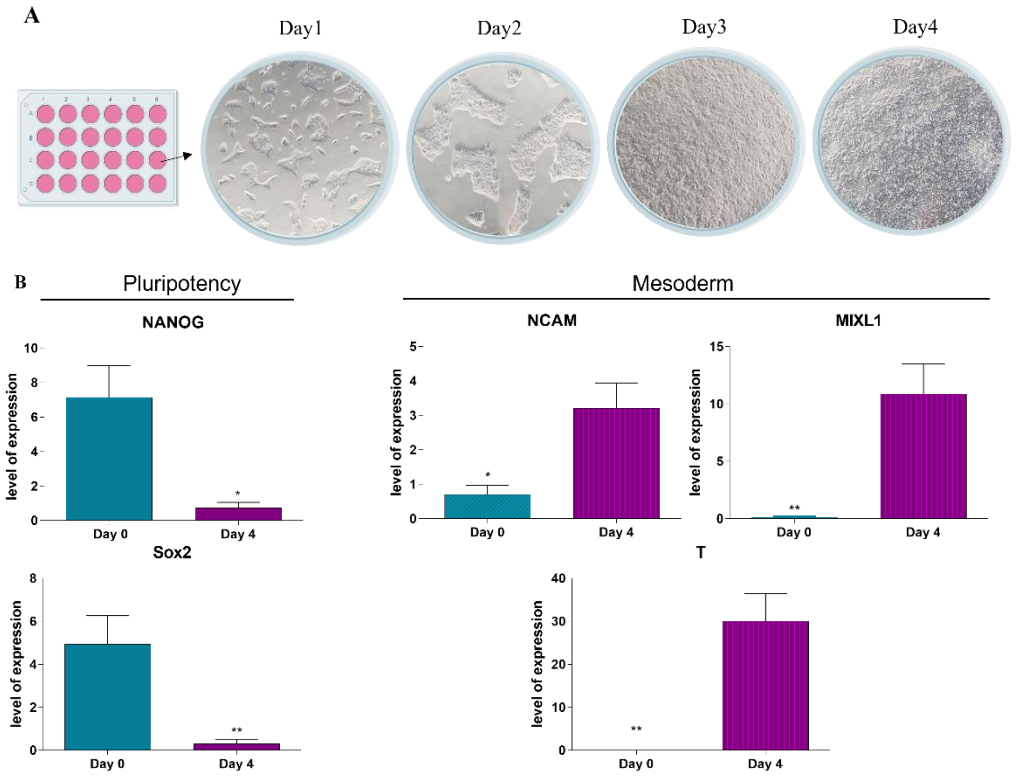

Figure 13.**Mesoderm differentiation**. A) Morphological changes during the early stages of the mesodermal differentiation protocol. B) Expression of undifferentiated cell markers (NANOG and Sox2) and early mesoderm markers (NCAM, MIXL1,T) measured by quantitative PCR (qPCR). While the expression level of pluripotency markers decreases, the expression of early mesoderm increases. The same result was observed for the control. Only the SDH derived iPSC data is shown. Statistical significance was calculated using Welch's test. $p \leq 0.05$, * $p \leq 0.01$. Each bar represents the mean value ± SEM.

3.2. Genetic inhibition of the SDH complex

Once the pluripotency status of the patient-derived iPSCs had been confirmed, different approaches to mimic the disease were employed. As a first step, the inactivation of the SDH gene was performed by using the gene-editing CRISPR/CAS9 approach. SDHA knockout in iPSCs derived from SDH-deficient patient would provide a valid model of the disease both because it reproduces the loss of the SDH complex and because the entire genetic background of the patient is retained. Hence, the CRISPR-Cas9 method was used with the aim of introducing a second mutation in the SDHA gene, in order to compare SDH -/- with SDH +/- iPSC. SDHA knockout was performed into both the genome of healthy donor iPSC (CNTR) and SDH-deficient patient iPSC (SDH iPSC). The CRISPR-Cas9 system that was used had a target-specific CRISPR RNA (crRNA), a Cas9 endonuclease and a transactivating crRNA (tracrRNA) conjugated with ATTO™ 550 fluorescent dye to the 5' end.

This allowed us to test the transfection efficiency after 24 hours. Following cytofluorimetric data analysis, the transfection efficiency of our study resulted to be of about 40% in all the experiments that were carried out. Overall a total of 120 clones were screened and collected in both experiments. Subsequently, the target region of Cas9 on the exon 9 of SDHA gene was sequenced by Sanger sequencing. The obtained results showed that around 50% of the clones reported a mutation on the target region, as evident in Figure 14A. A deletion of 8bp was the most recurrent mutation in all the selected clones (Figure 14B). These results enabled us to conclude that the adopted strategy is very efficient and precise, since it enabled us to introduce a mutation in the region of interest. Nevertheless, we also observed that the mutation was only introduced in heterozygosis, resulting in only one mutant allele. These results let us assume that a homozygotic mutation might most likely severely impair cell growth or survival. To attempt the identification of very rare knockout clones, cells were sorted as single cells by FACS analysis. However, the single cells selected and sequenced kept showing a wild type genotype.

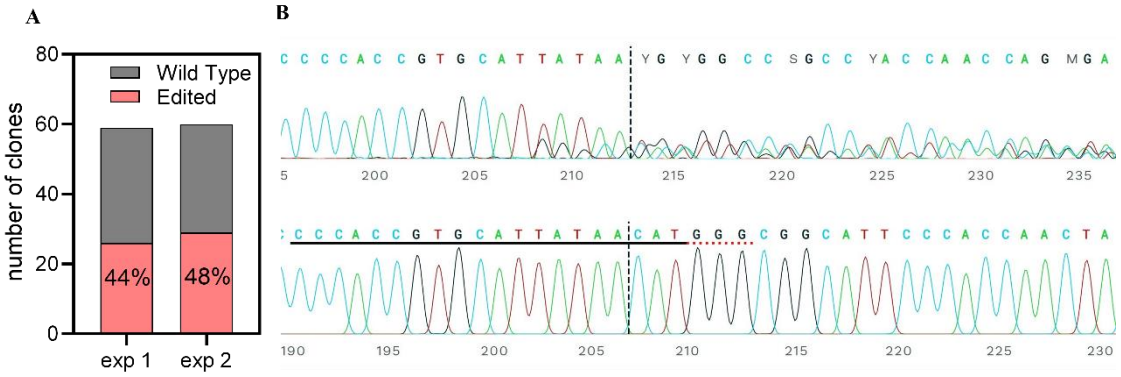

Figure 14.**Screening and sequencing of edited clones**. A) On the left, the percentage of edited and wild type clones in the two gene editing experiments. B)On the right, electropherograms derived from the Sanger sequencing of the mutation locus for an SDHA gene edited clone. (seq up: edited sample, seq down: control sample). The horizontal black underlined region represents the guide sequence. The horizontal red underline is the PAM site (Synthego's ICE analysis).

3.3. Chemical inhibition of the SDH complex

Since the gene editing experiments did not show a complete loss of the SDH gene, we opted to proceed with chemical inhibition of the SDH complex. Studying the effect of chemical inhibition of SDH is a promising starting point towards a better understanding of the effects caused by the loss

of such complex in vitro and to mimic the disease phenotype. Chemical inhibition experiments of the SDH complex were performed in both iPSC derived from healthy donors (CNTR iPSC) and iPSC derived from SDH-deficient patient (SDH iPSC) before and after the mesoderm differentiation. Specifically, cells were exposed for 24 hours with variable concentration (from 10 µM to 50 mM) of an SDHA inhibitor, 3-NPA. The use of specific assays allowed us to evaluate the effects of inhibition of the complex in terms of cytotoxicity and mitochondrial activity. We observed both an increase in cytotoxicity as drug concentrations increased as well as a decrease in mitochondrial activity at high concentrations. Both cell lines showed a strong reduction of mitochondrial activity at specific concentration of 3-NPA and IC50 ranging between 5 mM and 15 mM. The cell viability is maintained around 50% for the concentrations that are therapeutically active (5Mm-15mM) (Figure 15).

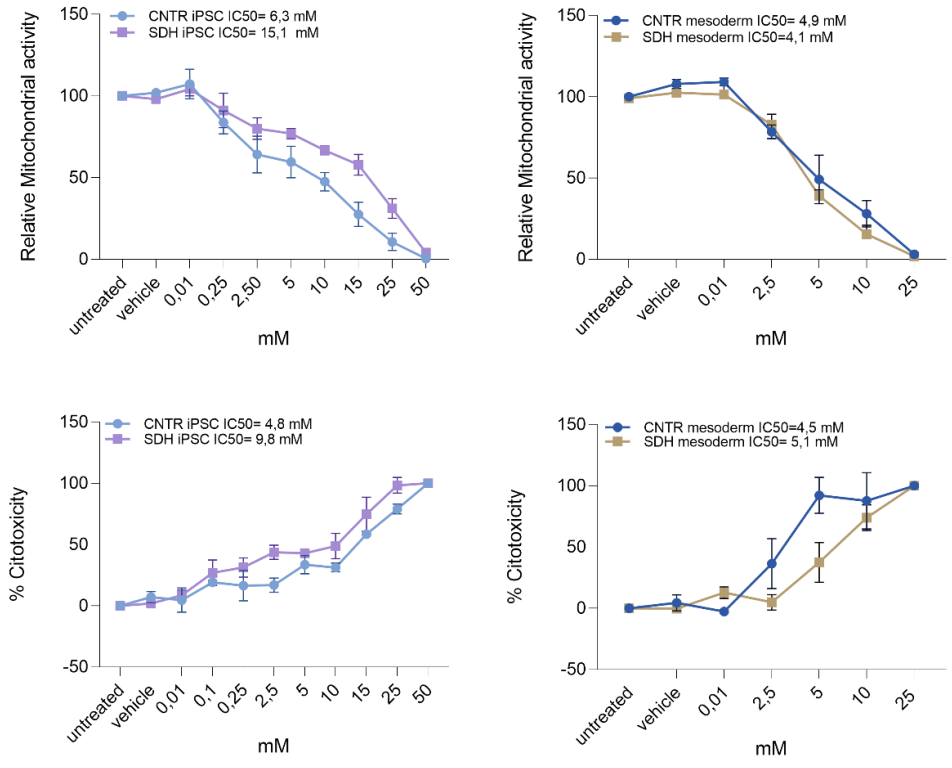

Figure 15.**Relative mitochondrial activity and cytotoxicity in both iPSCs/mesoderm cell lines**. Dose-response curves after 24h of 3-NPA treatment of healthy donors (CNTR iPSC) and iPSC derived from SDH deficient patient (SDH iPSC) before and after mesoderm differentiation (CNTR mesoderm and SDH mesoderm). An increase in cytotoxicity as drug concentrations increase and a decrease in mitochondrial activity at higher concentration was observed.

It is reasonable to hypothesise that the chemical inhibition of the SDHA subunit of the SDH complex in iPSC could lead to the degradation of the entire complex thus partially mimicking the disease phenotype. This approach was the starting point for investigating the expression levels of markers that we have shown to be modulated in SDH deficient GISTs. Q-PCRs were performed by comparing the untreated cells with the cells treated at the concentrations that effectively inhibited the SDH complex (Figure 16). The first set of genes analysed were those known to be linked to hypoxia signalling. The population exposed to 3-NPA showed a statistically significant upregulation of hypoxia-related markers such as HIF1α, EPAS1 (Endothelial PAS Domain Protein 1), VEGF compared to untreated cells, in both iPSC lines. These results confirm that the succinate accumulation, caused by the loss of function of the SDH complex, leads to a hypoxia status by altering the gene expression of hypoxia related markers. The same results are observed for cells differentiated towards the mesoderm. Subsequently, we investigated the expression level of a set of genes linked to the neural lineage commitment. In accordance with previous observations in our gene expression analysis of SDH and KIT mutant patients, the iPSCs treated with SDHA inhibitor showed a statistically significant increase of expression levels of neural markers. Interestingly, the expression of neural markers such as LHX2, CDH2 and NEFL were significant higher in exposed cells in both iPSCs and differentiated cells. Notably, the significantly increased expression of the marker IGF1R, a characteristic marker of SDH-deficient GISTs was also observed. Although there is no significance in CNTR iPSC, the increasing trend of this marker after the inhibition of the complex is evident. In conclusion, qPCR data, obtained by using the concentrations that effectively inhibit mitochondrial activity, showed that at concentrations ≥ 5mM, after 24 h of treatment, the molecular phenotypes typical of SDH-deficient GISTs are produced. In addition, these results lead us to the conclusion that the expression of neural markers is directly linked to the inactivation of the SDH complex and not to a different molecular origin of GISTs.

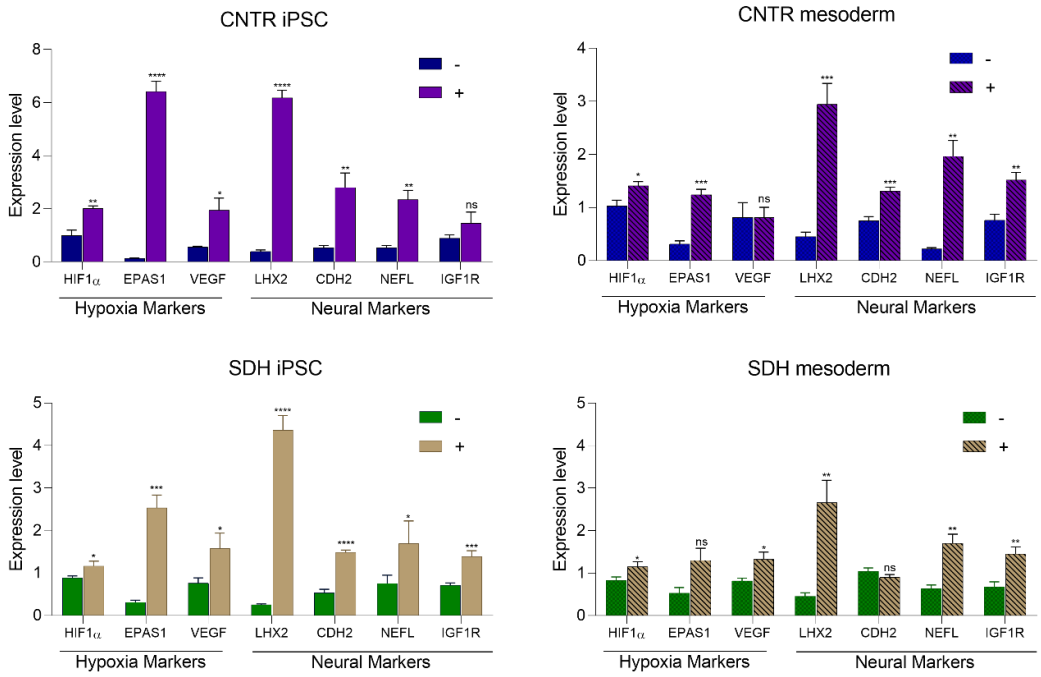

Figure.16.**Gene expression analysis in 3-NPA exposed cells**. Expression levels of the SDH-deficient GIST markers evaluated through qPCR after a 24h exposure with 3-NPA in Healthy donor iPSCs and mesoderm (CNTR iPSC, CNTR mesoderm), derived from SDH-deficient patient iPSC and mesoderm (SDH iPSC, SDH mesoderm); the expression of hypoxia and neural markers increase in both populations at high concentration of 3-NPA. Statistical significance was calculated comparing treated samples with untreated and using Welch's test.*$p \leq 0.05$, ** $p \leq 0.01$, *** $p \leq 0.001$, **** $p \leq 0.0001$, ns:not significant, (-) untreated, (+) treated. Each bar represents the mean value ± SEM.

DISCUSSION

This study was aimed at providing a comprehensive characterisation of SDH-deficient GIST, and in particular the SDHA-mutant subgroup, a rare tumour for which much information is still lacking. Despite the great improvements achieved in the last decades in the management of KIT/PDGFRA mutant patients, different aspects of the pathology and treatment of the SDH-deficient subgroup still remain unclear. The possibility of carrying out molecular investigations of both sequencing and gene expression was a remarkable resource for the understanding of this disease. In addition, the development of a pre-clinical model of a rare tumour, which is limited due to the small number of cases and therefore prevents large-scale analyses, is a valuable instrument that may provide us with useful information related to the pathogenesis and potential therapeutic targets. Firstly, the assessment of the germline SDHA status in our SDH-deficient GIST series highlighted that germline mutations in SDHA are highly frequent in SDHA-deficient GIST. Our findings showed high diversity of both the variant type and the position, confirming that SDHA can be inactivated by mutations scattered throughout its whole genomic sequence. This observations underscores the importance of the genetic analysis in qualified high-volume molecular diagnostic centres, as already suggested in other settings[79]. Specifically, we found seven truncating germline variants, seven germline missense variants and two cases leading to a predicted premature protein sequence truncation. Based on previous data, the most recurrent mutation is Arg31* variant, which was found in only one patient in our study [22,42,44-74, 67-70]. All the analysed patients carried two mutational events at the SDHA locus, supporting the two-hit model of tumor onco-suppressor genes inactivation. In our series, the presence of GIST in the context of *SDHA*-mutant GIST seemed very exclusive, indeed only one case reported having been affected by a different type of tumor (paraganglioma more than 10 years before). Furthermore, in accordance with previous studies, our analysis absolutely proves the highly relevant association between germline SDHA pathogenic variants and GIST onset[43,80,70,48,81]. The only study that up to now, suggested the possible role of SDHA as a predisposing factor for other tumor types, reported the development of neuroblastoma in one SDHA-mutation carrier showing the inactivation of the second allele[72]. Our series confirms the clinical aspects already known such as the stomach as the primary localisation, the indolent clinical course and long-term survival prognosis. However, the disease at onset presents a high heterogeneity both for the multifocality and metastatic presentation at diagnosis. In our study, 38% of the patients were older than 50 years, with peaks up to 70 years old highlighting that the disease may occur in older

adulthood[43,48,4,46,47]. These observations were also found in previous studies, and altogether have very important implications supporting the need for genetic counselling[49,43,70,48,82]. Indeed, even though the clinical findings indicate a low penetrance of SDHA mutation in affected families[7,83], the concept of a lifelong risk for GIST development requires genetic testing and permanent clinical surveillance of SDHA-variant carriers. A more functional approach based on the identification of comprehensive signalling pathways alterations that could be involved in tumor development in the context of SDH complex dysfunction are instrumental in better understanding the disease biology and potential molecular targets. To this purpose we focused on the molecular characterization of SDH-deficient GISTs, by using a retrospective collection of RNA-seq and microarray data to compare the gene expression profile of SDH-deficient and KIT-mutant GIST groups. In agreement with previous studies, we confirmed distinct pathways in the two subgroups[26] but also, we found new interesting signalling pathways characteristic of SDH-deficient GISTs. Our analysis showed that SDH-deficient subgroup are characterized by the upregulation of FGFR signalling, hypoxia, and EMT pathways. In addition, the SDH-deficient tumors exhibited an overexpression of neural markers. Conversely, among the under expressed pathways we found the interferon gamma/alpha response, KRAS and mTORC1 signalling, and fatty acid metabolism and complement. Interestingly, the immune-related signatures resulted under-represented compared to other GIST subgroups such as the PDGFRA-mutant GIST[77,78]. The analysis confirmed the expression of markers related to neural commitment such as LHX2, NEFL, KIRREL3, CDH2, and IGF1R. Moreover, our data revealed a high expression of other important neural markers such as the glutamate receptor GRIA1, the integrin-8 ITGA8, and the neuronal cell adhesion molecule NRCAM. These results lead us to suppose that the SDH-deficient GIST group originates from cells committed to the neural lineage. Considering the hypothesis of a different molecular origin, we further analyzed the expression of ICC markers in the two groups of samples. We realized that the majority of ICC markers were highly and equally expressed in both GIST subgroups; however, we found a modulated expression of some ICC markers know to be involved in the neuronal differentiation, such as THBS4 and EDN3. Intriguingly, an increased expression of THBS4 was demonstrated to induce neuronal differentiation in CSPG4- expressing neural progenitor cells[84]. On the contrary, EDN3 expression is related to the inhibition of neuronal differentiation[85]. It is known that ICCs derive from mesenchymal stem cells that keep KIT expression during smooth muscle differentiation, probably due to induction from the nearby neural crest cells in the primitive gut that will give rise to the enteric nervous system [86,87]. ICCs exhibit a relevant expression plasticity, which is probably reflected in their malignant

counterparts. Taken together, all these observations prompted us to suppose that SDH-deficient GISTs could originate from a different type of ICC polarized towards a cell type with more distinct neural features. Moreover, we found a differential expression profile in two groups for FGF ligands. In particular, FGF4, FGF2, FGF7, and FGF10 were significantly over expressed in the SDH-deficient group. The involvement of FGF/FGFR signalling to GIST pathogenesis was already observed. In particular, it has been shown that in SDH-deficient GISTs, methylation of an FGF insulator region is responsible for the induction of FGF4 expression[88,89]. FGF3–FGF4 locus topology is profoundly altered in SDH-deficient GISTs, with CTCF insulator loss allowing aberrant expression of FGFR ligand genes[58]. We also recently confirmed that overexpression of the FGF4 oncogene is a shared feature also of KIT/PDGFRA/SDH/RAS-P negative GIST[90]. Moreover, SDH deficient subgroup showed an up-regulation of genes encoding for the lysosomal enzymes, involved in the degradation of the main GAG groups. GAGs are a family of complex polysaccharides that interact with different growth factors and other transient components of the extra cellular matrix[91]. These molecules are involved in the promotion of the tumorigenic processes by controlling the signalling loops that leads to unregulated cell growth, cancer progression, angiogenesis, and metastasis[92]. Notably, specific groups of GAGs, such as the heparan sulfates, are able to trigger cell proliferation mechanisms through fibroblast growth factors (FGF1 and FGF2), vascular endothelial growth factor (VEGF), and transforming growth factor- signaling[92,93].Furthermore, we compared our GIST series with a set of SDH-deficient pheochromocytoma/ paraganglioma with the aim to understand whether the molecular signature of SDH-deficient GISTs was distinctive of GIST or associated to the SDH complex deficiency. Our observations indicate that the expression of EMT, hedgehog, and hypoxia pathways is strongly linked to the loss of the SDH complex, a feature shared with pheochromocytoma/paraganglioma, which could explain and support the clinical differences with other GIST subgroups, such as for the metastatic behaviour. The SDH-deficient GIST series showed a high expression level of several genes linked to EMT signature such as the cadherins CDH2 and CDH6, the cytokine receptor CRLF1, the secretory protein SCG2, the amyloid precursor APLP1, the enolase ENO2, and the secreted protein MGP. A transcriptional profiling study about the participation of EMT signature in the metastatic evolution of pheochromocytoma/paraganglioma identified pathways that distinguish SDHB-metastatic from all other types of pheochromocytoma/ paraganglioma. Therefore, the activation of the EMT process might be associated to the invasive phenotype of this group of tumors[94]. Our cluster analysis showed a separation of SDH-deficient GISTs together with pheochromocytoma/paraganglioma from KIT-mutant GISTs, suggesting that

this pattern is common for those tumors sharing the loss of SDH complex. A similar analysis showed that also the genes related to hypoxia signaling cluster together in SDH-deficient GISTs and pheochromocytoma/paraganglioma, separating from KIT-mutant GISTs. Hypoxia is a metabolic condition of low oxygen level in the tissues and it is directly implicated in the neoplastic transformation of cells. However, the hypoxia-induced phenotypes are observed in some tumors also in the absence of hypoxia; in these cases, it is referred to as pseudo-hypoxia. Several malignant features are associated with the hypoxic/pseudo-hypoxic condition, including stem cell-like trait, metabolic alterations, and EMT as well as angiogenesis, invasion, metastasis[95]. In this study, the immunological state of both groups of GISTs was evaluated. Our results showed that SDH-deficient GISTs are noninflamed cancers with a poor tumor microenvironment and definitely different from other GIST groups. In fact, we found a significant absence of tumor-infiltrating CD8+, M1 macrophages, NK cells, and dendritic cells in SDH deficient GISTs. Moreover, the EIIS signature in SDH-deficient GISTs is lower than in KIT-mutant GISTs. By comparing the TIS score in our GIST series with the TIS score distribution in several tumor types (collected in TCGA database), we observed that the SDH-deficient TIS score is closer to that of cold tumors (glioblastoma multiforme, kidney renal papillary cell carcinoma) with respect to other GIST molecular subgroups (both KIT-mutant and PDGFRA-mutant) that showed a TIS score more similar to hot tumors (such as melanoma and lung cancer).

It is known that SDH-deficient GIST lack clinically effective TKIs due to the absence of a tyrosine kinase oncogenic driver mutation; moreover, the lack of appropriate cellular models further hamper the possibility to test and predict the efficacy of pharmacological compounds in a preclinical setting. We focused on the development of a preclinical model by using pluripotent stem cells, which were obtained from adult cells of mutant SDHA patient. We were able to effectively differentiate cells towards the mesoderm lineage, obtaining cell populations that express the early mesoderm genes T, MIXL1, and NCAM. In addition we used different approaches to genetically inhibit the SDH complex. We first made use of the CRISPR/Cas9 technology to precisely knockout the SDHA gene , but the knockout of both SDHA alleles could affect or impair cell viability. On the other hand, the development of chemical inhibition strategies of the SDH complex enabled us to reproduce the biochemical and molecular mechanisms involved in tumour development. We effectively inhibited the subunit A of the SDH complex with 3-NPA treatment by observing a simultaneous decrease in mitochondrial respiration. Beyond the accumulation of succinate[96] it has been shown that decreased

mitochondrial respiration has been identified as a metabolic phenotype of SDH knockout and mutant cells[97, 98,99]. The cytotoxicity was assessed by quantifying the accumulation of LDH that results from cellular damage. It is important to highlight that LDH quantitation is influenced by the metabolic pathway that has been inhibited and could therefore be overestimated since LDH expression is induced when the mitochondrial activity is inhibited. Therefore, we can assume that the cytotoxicity of this treatment is lower than the calculated one. Q-PCR analysis in our iPSC model of genes related to hypoxia and neural commitment leads us to hypothesize that the loss of function of SDH complex is directly involved in this two signalling pathways, namely hypoxia and neural differentiation. In fact, we observed a high significance in the upregulation of hypoxia-related genes such as VEGF, HIF1α, EPAS1 and genes related to the neural commitment such as LHX2, CDH2, NEFL, IGF1R in 3-NPA treated cells. These data confirm the potential of the iPSC model in reproducing at the cellular level the disease phenotype suggesting that the loss of SDH activity is sufficient to drive the metabolic phenotype of SDH mutant tumors. The easy manipulation and high reliability of the iPSC model warrants further investigations on the signalling pathways evoked by SDH loss of function and on novel and repurposed pharmacological approaches in this GIST subgroup still orphan of specific targeted treatments.

CONCLUSION

Overall, our study provided a comprehensive representation of clinical and molecular information of SDH-deficient GIST. We delved into the expression landscape of SDH-deficient GISTs highlighting gene expression pattern similarity and differences comparing to the most common KIT-mutant GISTs and to other neoplasm carrying an analogous molecular background leading to the SDH loss of function. Moreover, we provided evidence that iPSC model has the potential to mimic the phenotype of the disease. In fact, we proved that the chemical inhibition of SDHA in an iPSC model was sufficient to effectively reduce mitochondrial respiration and to reproduce the metabolic and molecular phenotype of tumors associated with SDH mutations. We also observed that SDHA-mutant GIST patients are almost exclusively germline SDHA-variant carriers that are predisposed to develop the tumor throughout their entire life, and not just in early adulthood. Thus, the genetic counselling of SDHA-variant carriers and relatives should be planned and their clinical follow-up should be accurately defined. Taken together, these findings contribute to enrich the knowledge about the biology of this tumor and, consequently, provide effective information for new therapeutic strategies.

REFERENCES

1. Kindblom, L. G., Remotti, H. E., Aldenborg, F. & Meis-Kindblom, J. M. Gastrointestinal pacemaker cell tumor (GIPACT): Gastrointestinal stromal tumors show phenotypic characteristics of the interstitial cells of Cajal. *Am. J. Pathol.* (1998).

2. Isozaki, K. & Hirota, S. Gain-of-Function Mutations of Receptor Tyrosine Kinases in Gastrointestinal Stromal Tumors. *Curr. Genomics* (2006) doi:10.2174/138920206779315755.

3. Heinrich, M. C. *et al.* PDGFRA activating mutations in gastrointestinal stromal tumors. *Science (80-.).* (2003) doi:10.1126/science.1079666.

4. Pantaleo, M. A. *et al.* Analysis of all subunits, SDHA, SDHB, SDHC, SDHD, of the succinate dehydrogenase complex in KIT/PDGFRA wild-type GIST. *Eur. J. Hum. Genet.* (2014) doi:10.1038/ejhg.2013.80.

5. Janeway, K. A. *et al.* Defects in succinate dehydrogenase in gastrointestinal stromal tumors lacking KIT and PDGFRA mutations. *Proc. Natl. Acad. Sci. U. S. A.* (2011) doi:10.1073/pnas.1009199108.

6. Carney, J. A. & Stratakis, C. A. Familial paraganglioma and gastric stromal sarcoma: A new syndrome distinct from the Carney triad. *Am. J. Med. Genet.* (2002) doi:10.1002/ajmg.10235.

7. Recht, H. S. & Fishman, E. K. Carney-Stratakis syndrome: A dyad of familial paraganglioma and gastrointestinal stromal tumor. *Radiol. Case Reports* (2020) doi:10.1016/j.radcr.2020.08.002.

8. Miettinen, M. & Lasota, J. Succinate dehydrogenase deficient gastrointestinal stromal tumors (GISTs) - A review. *International Journal of Biochemistry and Cell Biology* vol. 53 514–519 (2014).

9. Nilsson, B. *et al.* Gastrointestinal stromal tumors: The incidence, prevalence, clinical course, and prognostication in the preimatinib mesylate era - A population-based study in western Sweden. *Cancer* (2005) doi:10.1002/cncr.20862.

10. Søreide, K. *et al.* Global epidemiology of gastrointestinal stromal tumours (GIST): A systematic review of population-based cohort studies. *Cancer Epidemiology* (2016) doi:10.1016/j.canep.2015.10.031.

11. Charville, G. W. & Longacre, T. A. Surgical Pathology of Gastrointestinal Stromal Tumors: Practical Implications of Morphologic and Molecular Heterogeneity for Precision Medicine. *Advances in Anatomic Pathology* (2017) doi:10.1097/PAP.0000000000000166.

12. Fülöp, E., Marcu, S., Milutin, D. & Borda, A. Gastrointestinal stromal tumors: Review on morphology, diagnosis and management. *Romanian Journal of Morphology and Embryology* (2008).

13. Loughrey, M. B. *et al.* KIT immunohistochemistry and mutation status in gastrointestinal stromal tumours (GISTs) evaluated for treatment with imatinib. *Histopathology* (2006) doi:10.1111/j.1365-2559.2006.02464.x.

14. El-Menyar, A., Mekkodathil, A. & Al-Thani, H. Diagnosis and management of gastrointestinal stromal tumors: An up-to-date literature review. *Journal of Cancer Research and Therapeutics* (2017) doi:10.4103/0973-1482.177499.

15. Miettinen, M., Sobin, L. H. & Lasota, J. Gastrointestinal stromal tumors of the stomach: A clinicopathologic, immunohistochemical, and molecular genetic study of 1765 cases with long-term follow-up. *Am. J. Surg. Pathol.* (2005) doi:10.1097/01.pas.0000146010.92933.de.

16. Miettinen, M., Makhlouf, H., Sobin, L. H. & Lasota, J. Gastrointestinal stromal tumors of the jejunum and ileum: A clinicopathologic, immunohistochemical, and molecular genetic study of 906 cases before imatinib with long-term follow-up. *Am. J. Surg. Pathol.* (2006) doi:10.1097/00000478-200604000-00008.

17. DeMatteo, R. P. *et al.* Two hundred gastrointestinal stromal tumors: Recurrence patterns and prognostic factors for survival. *Ann. Surg.* (2000) doi:10.1097/00000658-200001000-00008.

18. Hirota, S. *et al.* Gain-of-Function Mutations of c-kit in Human Gastrointestinal Stromal Tumors Seiichi Hirota ,* Koji Isozaki ,* Yasuhiro Moriyama. *Science (80-.).* (1998).

19. Lasota, J. *et al.* Gastrointestinal Stromal Tumors with Internal Tandem Duplications in 3′ End of KIT Juxtamembrane Domain Occur Predominantly in Stomach and Generally Seem to Have a Favorable Course. *Mod. Pathol.* (2003) doi:10.1097/01.MP.0000097365.72526.3E.

20. Lasota, J. *et al.* Clinicopathologic profile of gastrointestinal stromal tumors (GISTs) with primary KIT exon 13 or exon 17 mutations: A multicenter study on 54 cases. *Mod. Pathol.* (2008) doi:10.1038/modpathol.2008.2.

21. Ahmed, M. Recent advances in the management of gastrointestinal stromal tumor. *World J. Clin. Cases* (2020) doi:10.12998/WJCC.V8.I15.3142.

22. Kim, S. Y. & Kim, K. O. Management of gastric subepithelial tumors: The role of endoscopy. *World J. Gastrointest. Endosc.* (2016) doi:10.4253/wjge.v8.i11.418.

23. Boikos, S. A. *et al.* Molecular subtypes of KIT/PDGFRA wild-type gastrointestinal stromal tumors a report from the national institutes of health gastrointestinal stromal tumor clinic. *JAMA Oncol.* (2016) doi:10.1001/jamaoncol.2016.0256.

24. Miettinen, M. *et al.* Succinate Dehydrogenase-Deficient GISTs. *Am. J. Surg. Pathol.* (2011) doi:10.1097/pas.0b013e3182260752.

25. Pantaleo, M. A., Nannini, M., Corless, C. L. & Heinrich, M. C. Quadruple wild-type (WT) GIST: Defining the subset of GIST that lacks abnormalities of KIT, PDGFRA, SDH, or RAS signaling pathways. *Cancer Med.* (2015) doi:10.1002/cam4.325.

26. Nannini, M. *et al.* Integrated genomic study of quadruple-WT GIST

(KIT/PDGFRA/SDH/RAS pathway wild-type GIST). *BMC Cancer* (2014) doi:10.1186/1471-2407-14-685.

27. Fletcher, C. D. M. *et al.* Diagnosis of gastrointestinal stromal tumors: A consensus approach. *Hum. Pathol.* (2002) doi:10.1053/hupa.2002.123545.

28. Miettinen, M. & Lasota, J. Gastrointestinal stromal tumors: Pathology and prognosis at different sites. *Semin. Diagn. Pathol.* (2006) doi:10.1053/j.semdp.2006.09.001.

29. Judson, I. *et al.* UK clinical practice guidelines for the management of gastrointestinal stromal tumours (GIST). *Clin. Sarcoma Res.* (2017) doi:10.1186/s13569-017-0072-8.

30. Wozniak, A. *et al.* Tumor genotype is an independent prognostic factor in primary gastrointestinal stromal tumors of gastric origin: A European multicenter analysis based on ConticaGIST. *Clin. Cancer Res.* (2014) doi:10.1158/1078-0432.CCR-14-1677.

31. Joensuu, H. *et al.* One vs three years of adjuvant imatinib for operable gastrointestinal stromal tumor: A randomized trial. *JAMA - J. Am. Med. Assoc.* (2012) doi:10.1001/jama.2012.347.

32. Verweij, J. *et al.* Progression-free survival in gastrointestinal stromal tumours with high-dose imatinib: Randomised trial. *Lancet* (2004) doi:10.1016/S0140-6736(04)17098-0.

33. Demetri, G. D. *et al.* Efficacy and safety of sunitinib in patients with advanced gastrointestinal stromal tumour after failure of imatinib: a randomised controlled trial. *Lancet* (2006) doi:10.1016/S0140-6736(06)69446-4.

34. Thigpen, J. T. Efficacy and safety of regorafenib for advanced gastrointestinal stromal tumours after failure of imatinib and sunitinib (GRID): an international, multicentre, randomised, placebo-controlled, phase 3 trial. *Yearb. Oncol.* (2013) doi:10.1016/j.yonc.2013.07.007.

35. Mullady, D. K. & Tan, B. R. A multidisciplinary approach to the diagnosis and treatment of

gastrointestinal stromal tumor. *Journal of Clinical Gastroenterology* (2013) doi:10.1097/MCG.0b013e3182936c87.

36. Bezawork-Geleta, A., Rohlena, J., Dong, L., Pacak, K. & Neuzil, J. Mitochondrial Complex II: At the Crossroads. *Trends in Biochemical Sciences* (2017) doi:10.1016/j.tibs.2017.01.003.

37. Barletta, J. A. & Hornick, J. L. Succinate dehydrogenase-deficient tumors: Diagnostic advances and clinical implications. *Advances in Anatomic Pathology* (2012) doi:10.1097/PAP.0b013e31825c6bc6.

38. Kosmider, O. *et al.* Mutations of IDH1 and IDH2 genes in early and accelerated phases of myelodysplastic syndromes and MDS/myeloproliferative neoplasms. *Leukemia* (2010) doi:10.1038/leu.2010.52.

39. Miettinen, M. *et al.* Succinate dehydrogenase-deficient GISTs: A clinicopathologic, immunohistochemical, and molecular genetic study of 66 gastric GISTs with predilection to young age. *Am. J. Surg. Pathol.* (2011) doi:10.1097/PAS.0b013e3182260752.

40. Pantaleo, M. A. *et al.* Good survival outcome of metastatic SDH-deficient gastrointestinal stromal tumors harboring SDHA mutations. *Genet. Med.* (2015) doi:10.1038/gim.2014.115.

41. Pasini, B. *et al.* Clinical and molecular genetics of patients with the Carney-Stratakis syndrome and germline mutations of the genes coding for the succinate dehydrogenase subunits SDHB, SDHC, and SDHD. *Eur. J. Hum. Genet.* (2008) doi:10.1038/sj.ejhg.5201904.

42. Aidan Carney, J. Gastric stromal sarcoma, pulmonary chondroma, and extra-adrenal paraganglioma (Carney triad): Natural history, adrenocortical component, and possible familial occurrence. *Mayo Clin. Proc.* (1999) doi:10.4065/74.6.543.

43. Miettinen, M. *et al.* Immunohistochemical loss of succinate dehydrogenase subunit a (SDHA) in gastrointestinal stromal tumors (GISTs) signals SDHA germline mutation. *Am. J. Surg.*

Pathol. (2013) doi:10.1097/PAS.0b013e3182671178.

44. Belinsky, M. G., Rink, L. & von Mehren, M. Succinate dehydrogenase deficiency in pediatric and adult gastrointestinal stromal tumors. *Frontiers in Oncology* (2013) doi:10.3389/fonc.2013.00117.

45. Bannon, A. E. *et al.* Biochemical, molecular, and clinical characterization of succinate dehydrogenase subunit A variants of unknown significance. *Clin. Cancer Res.* (2017) doi:10.1158/1078-0432.CCR-17-1397.

46. Italiano, A. *et al.* SDHA loss of function mutations in a subset of young adult wild-type gastrointestinal stromal tumors. *BMC Cancer* (2012) doi:10.1186/1471-2407-12-408.

47. Dwight, T. *et al.* Loss of SDHA expression identifies SDHA mutations in succinate dehydrogenase-deficient gastrointestinal stromal tumors. *Am. J. Surg. Pathol.* (2013) doi:10.1097/PAS.0b013e3182671155.

48. Oudijk, L. *et al.* SDHA mutations in adult and pediatric wild-type gastrointestinal stromal tumors. *Mod. Pathol.* (2013) doi:10.1038/modpathol.2012.186.

49. Wagner, A. J. *et al.* Loss of expression of SDHA predicts SDHA mutations in gastrointestinal stromal tumors. *Mod. Pathol.* (2013) doi:10.1038/modpathol.2012.153.

50. McWhinney, S. R., Pasini, B. & Stratakis, C. A. Familial Gastrointestinal Stromal Tumors and Germ-Line Mutations. *N. Engl. J. Med.* (2007) doi:10.1056/nejmc071191.

51. Killian, J. K. *et al.* Succinate dehydrogenase mutation underlies global epigenomic divergence in gastrointestinal stromal tumor. *Cancer Discov.* (2013) doi:10.1158/2159-8290.CD-13-0092.

52. Urbini, M. *et al.* SDHC methylation in gastrointestinal stromal tumors (GIST): A case report. *BMC Med. Genet.* (2015) doi:10.1186/s12881-015-0233-7.

53. Selak, M. A. *et al.* Succinate links TCA cycle dysfunction to oncogenesis by inhibiting HIF-α prolyl hydroxylase. *Cancer Cell* (2005) doi:10.1016/j.ccr.2004.11.022.

54. Nannini, M. *et al.* Expression of IGF-1 receptor in KIT/PDGF receptor-α wild-type gastrointestinal stromal tumors with succinate dehydrogenase complex dysfunction. *Futur. Oncol.* (2013) doi:10.2217/fon.12.170.

55. C., B. *et al.* Gene expression of the IGF pathway family distinguishes subsets of gastrointestinal stromal tumors wild type for KIT and PDGFRA. *Cancer Med.* (2013).

56. Pantaleo, M. A. *et al.* Insulin-like growth factor 1 receptor expression in wild-type GISTs: A potential novel therapeutic target. *Int. J. Cancer* (2009) doi:10.1002/ijc.24595.

57. Morin, A. *et al.* TET-Mediated Hypermethylation Primes SDH-Deficient Cells for HIF2α-Driven Mesenchymal Transition. *Cell Rep.* (2020) doi:10.1016/j.celrep.2020.03.022.

58. Flavahan, W. A. *et al.* Altered chromosomal topology drives oncogenic programs in SDH-deficient GISTs. *Nature* (2019) doi:10.1038/s41586-019-1668-3.

59. Murray, M. *et al.* Treatment of wild-type gastrointestinal stromal tumor (WT-GIST) with imatinib and sunitinib. *Pediatr. Blood Cancer* (2008) doi:10.1002/pbc.21312.

60. Ben-Ami, E. *et al.* Long-term follow-up results of the multicenter phase II trial of regorafenib in patients with metastatic and/or unresectable GI stromal tumor after failure of standard tyrosine kinase inhibitor therapy. *Ann. Oncol.* (2016) doi:10.1093/annonc/mdw228.

61. Ganjoo, K. N. *et al.* A multicenter phase II study of pazopanib in patients with advanced gastrointestinal stromal tumors (GIST) following failure of at least imatinib and sunitinib. *Ann. Oncol.* (2014) doi:10.1093/annonc/mdt484.

62. Rossari, F., Minutolo, F. & Orciuolo, E. Past, present, and future of Bcr-Abl inhibitors: From chemical development to clinical efficacy. *Journal of Hematology and Oncology* (2018)

doi:10.1186/s13045-018-0624-2.

63. Pantaleo, M. A. *et al.* Impressive long-term disease stabilization by nilotinib in two pretreated patients with KIT/PDGFRA wild-type metastatic gastrointestinal stromal tumours. *Anticancer. Drugs* (2012) doi:10.1097/CAD.0b013e328352cc50.

64. Von Mehren, M. *et al.* Linsitinib (OSI-906) for the treatment of adult and pediatric wild-type gastrointestinal stromal tumors, a SARC phase II study. *Clin. Cancer Res.* (2020) doi:10.1158/1078-0432.CCR-19-1069.

65. Glod, J. *et al.* A Phase II trial of vandetanib in children and adults with succinate dehydrogenase-deficient gastrointestinal stromal tumor. *Clin. Cancer Res.* (2019) doi:10.1158/1078-0432.CCR-19-0986.

66. Demetri, G. D. *et al.* NCCN task force report: Update on the management of patients with gastrointestinal stromal tumors. *JNCCN Journal of the National Comprehensive Cancer Network* (2010) doi:10.6004/jnccn.2010.0116.

67. Li, B., Ruotti, V., Stewart, R. M., Thomson, J. A. & Dewey, C. N. RNA-Seq gene expression estimation with read mapping uncertainty. *Bioinformatics* (2009) doi:10.1093/bioinformatics/btp692.

68. Pantaleo, M. A. *et al.* Immune microenvironment profiling of gastrointestinal stromal tumors (GIST) shows gene expression patterns associated to immune checkpoint inhibitors response. *Oncoimmunology* (2019) doi:10.1080/2162402X.2019.1617588.

69. Carrera, S. *et al.* Germline c.1A>C heterozygous pathogenic variant in SDHA reported for the first time in a young adult with a gastric gastrointestinal stromal tumour (GIST): A case report. *Hered. Cancer Clin. Pract.* (2019) doi:10.1186/s13053-019-0124-6.

70. Belinsky, M. G. *et al.* Overexpression of insulin-like growth factor 1 receptor and frequent mutational inactivation of SDHA in wild-type SDHB-negative gastrointestinal stromal

tumors. *Genes Chromosom. Cancer* (2013) doi:10.1002/gcc.22023.

71. Jiang, Q. *et al.* A novel germline mutation in SDHA identified in a rare case of gastrointestinal stromal tumor complicated with renal cell carcinoma. *Int. J. Clin. Exp. Pathol.* (2015).

72. Gault, M. D. *et al.* Germline SDHA mutations in children and adults with cancer. *Cold Spring Harb. Mol. Case Stud.* (2018) doi:10.1101/mcs.a002584.

73. Pantaleo, M. A. *et al.* Differential expression of neural markers in KIT and PDGFRA wild-type gastrointestinal stromal tumours. *Histopathology* (2011) doi:10.1111/j.1365-2559.2011.04071.x.

74. Francavilla, C. *et al.* The binding of NCAM to FGFR1 induces a specific cellular response mediated by receptor trafficking. *J. Cell Biol.* (2009) doi:10.1083/jcb.200903030.

75. Ribatti, D., Tamma, R. & Annese, T. Epithelial-Mesenchymal Transition in Cancer: A Historical Overview. *Translational Oncology* (2020) doi:10.1016/j.tranon.2020.100773.

76. Hu, H. *et al.* Hypoxia-inducible factors enhance glutamate signaling in cancer cells. *Oncotarget* (2014) doi:10.18632/oncotarget.2593.

77. Vitiello, G. A. *et al.* Differential immune profiles distinguish the mutational subtypes of gastrointestinal stromal tumor. *J. Clin. Invest.* (2019) doi:10.1172/JCI124108.

78. Indio, V. *et al.* Gene Expression Profiling of PDGFRA Mutant GIST Reveals Immune Signatures as a Specific Fingerprint of D842V Exon 18 Mutation. *Front. Immunol.* (2020) doi:10.3389/fimmu.2020.00851.

79. Astolfi, A. *et al.* Targeted Deep Sequencing Uncovers Cryptic KIT Mutations in KIT/PDGFRA/SDH/RAS-P Wild-Type GIST. *Front. Oncol.* (2020) doi:10.3389/fonc.2020.00504.

80. Tufton, N., Sahdev, A., Drake, W. M. & Akker, S. A. Can subunit-specific phenotypes guide surveillance imaging decisions in asymptomatic SDH mutation carriers? *Clinical Endocrinology* (2019) doi:10.1111/cen.13877.

81. Pantaleo, M. A. *et al.* SDHA loss-of-function mutations in KIT-PDGFRA wild-type gastrointestinal stromal tumors identified by massively parallel sequencing. *J. Natl. Cancer Inst.* (2011) doi:10.1093/jnci/djr130.

82. Boikos, S. A. *et al.* Molecular Subtypes of KIT/PDGFRA Wild-Type Gastrointestinal Stromal Tumors . *JAMA Oncol.* (2016) doi:10.1001/jamaoncol.2016.0256.

83. Gill, A. J. Succinate dehydrogenase (SDH)-deficient neoplasia. *Histopathology* (2018) doi:10.1111/his.13277.

84. Yang, H. J. *et al.* Thrombospondin-4 Promotes Neuronal Differentiation of NG2 Cells via the ERK/MAPK Pathway. *J. Mol. Neurosci.* (2016) doi:10.1007/s12031-016-0845-1.

85. Lee, M. Y. *et al.* Transcriptome of interstitial cells of Cajal reveals unique and selective gene signatures. *PLoS One* (2017) doi:10.1371/journal.pone.0176031.

86. Radenkovic, G., Radenkovic, D. & Velickov, A. Development of interstitial cells of Cajal in the human digestive tract as the result of reciprocal induction of mesenchymal and neural crest cells. *Journal of Cellular and Molecular Medicine* (2018) doi:10.1111/jcmm.13375.

87. Pasternak, A., Szura, M., Gil, K. & Matyja, A. Interstitial cells of Cajal-systematic review. *Folia Morphologica (Poland)* (2016) doi:10.5603/FM.a2016.0002.

88. Itoh, N. & Ornitz, D. M. Evolution of the Fgf and Fgfr gene families. *Trends in Genetics* (2004) doi:10.1016/j.tig.2004.08.007.

89. Astolfi, A., Pantaleo, M. A., Indio, V., Urbini, M. & Nannini, M. The emerging role of the FGF/FGFR pathway in gastrointestinal stromal tumor. *International Journal of Molecular*

Sciences (2020) doi:10.3390/ijms21093313.

90. Urbini, M. *et al.* Gene duplication, rather than epigenetic changes, drives FGF4 overexpression in KIT/PDGFRA/SDH/RAS-P WT GIST. *Sci. Rep.* (2020) doi:10.1038/s41598-020-76519-y.

91. Vlcek, J. R., Reynolds, M. M. & Kipper, M. J. Enzymatic Degradation of Glycosaminoglycans and Proteoglycan-Mimetic Materials in Solution and on Polyelectrolyte Multilayer Surfaces. *Biomacromolecules* (2021) doi:10.1021/acs.biomac.1c00720.

92. Afratis, N. *et al.* Glycosaminoglycans: Key players in cancer cell biology and treatment. *FEBS Journal* (2012) doi:10.1111/j.1742-4658.2012.08529.x.

93. Morla, S. Glycosaminoglycans and glycosaminoglycan mimetics in cancer and inflammation. *International Journal of Molecular Sciences* (2019) doi:10.3390/ijms20081963.

94. Loriot, C. *et al.* Epithelial to mesenchymal transition is activated in metastatic pheochromocytomas and paragangliomas caused by SDHB gene mutations. *J. Clin. Endocrinol. Metab.* (2012) doi:10.1210/jc.2011-3437.

95. Kluckova, K. & Tennant, D. A. Metabolic implications of hypoxia and pseudohypoxia in pheochromocytoma and paraganglioma. *Cell and Tissue Research* (2018) doi:10.1007/s00441-018-2801-6.

96. Morin, A., Letouzé, E., Gimenez-Roqueplo, A. P. & Favier, J. Oncometabolites-driven tumorigenesis: From genetics to targeted therapy. *International Journal of Cancer* (2014) doi:10.1002/ijc.29080.

97. Rapizzi, E. *et al.* Role of microenvironment on neuroblastoma SK-N-AS SDHB-silenced cell metabolism and function. *Endocr. Relat. Cancer* (2015) doi:10.1530/ERC-14-0479.

98. Cardaci, S. *et al.* Pyruvate carboxylation enables growth of SDH-deficient cells by supporting

aspartate biosynthesis. *Nat. Cell Biol.* (2015) doi:10.1038/ncb3233.

99. Saxena, N. *et al.* SDHB-Deficient Cancers: The Role of Mutations That Impair Iron Sulfur Cluster Delivery. *J. Natl. Cancer Inst.* (2016) doi:10.1093/jnci/djv287.